Crustal architecture and evolution of the southwestern South China Sea: Implications to continental breakup

Sung-Ping Chang, Manuel Pubellier, Matthias Delescluse, Yan Qiu, Michael Nirrengarten, Geoffroy Mohn, Nicolas Chamot-Rooke, Yao Liang

Crustal architecture and evolution of the southwestern South China Sea: implications to continental breakup

Sung-Ping Chang [a], Manuel Pubellier [a], Matthias Delescluse [a], Yan Qiu [b], Michael Nirrengarten [c], Geoffroy Mohn [c], Nicolas Chamot-Rooke [a], Yao Liang [d]

[a] Ecole normale superieure, PSL Research University, CNRS UMR 8538, Laboratoire de Géologie, France

[b] Guangzhou Marine Geological Survey, Guangzhou, P.R. China

[c] Département Géosciences et Environnement, CY Cergy Paris University, France

[d] Key Laboratory of Petroleum Resources Research, Institute of Geology and Geophysics, Chinese Academy of Sciences, Beijing, China

Abstract

The South China Sea (SCS) is a marginal basin characterized by propagating breakup and subsequent seafloor spreading during the Cenozoic. Our study investigates the crustal architecture and tectonic evolution of the Xisha Islands - Northwest Borneo conjugate margins using a 1000 km long seismic profile and two shorter seismic lines. This system is characterized by wide margins showing a succession of rift basins with thinned continental crust, associated with large extensional detachment faults soling on top of the lower crust. In relation with crustal extension, several syn-rift sequences have been identified. The lower syn-rift unit (syn-rift I) shows well expressed wedge-shape growth strata. The upper one (syn-rift II) presents a more uniform thickness, and is slightly offset by normal faults dipping toward the depocenters. To illustrate the evolution of the southwestern SCS margins during continental breakup, we restore two conjugate sections near the oceanic magnetic anomaly C5En (18.8 Ma). The conjugate COT presents an asymmetrical hyper-extension architecture in cross sections, with the southern margin being the lower plate margin. In map view, the spatial variation of crustal structures illustrates a bayonet shape characterized by an initial N-S extension coeval with the first phase of seafloor spreading in the east sub-basin in the SCS. The extension direction

changed shortly later (circa 23Ma) to NW-SE opening in the southwest sub-basin in relation to a ridge jump. We suggest that variable extension direction is linked to changes in the compressional tectonic regime along Borneo and Palawan.

Keywords: Conjugate rifted margins; South China Sea margin; breakup process

1 Introduction

Continental extension and lithospheric breakup are transient processes controlling crustal thinning, sedimentary architectures and magmatic budget at passive rifted margins. The increase in quality of deep seismic profiles across examples of rifted margins provided critical new constrains on rift basin architecture, crustal structure and magmatic additions (e.g., Reston, 2009; Sutra et al., 2013; Tugend et al., 2018). These new datasets highlighted the important structural variability between distinct conjugate margins (e.g., Ranero and Pérez-Gussinyé, 2010, Brune et al. 2017; Sapin et al. 2021) but even across (Franke 2013, Nirrengarten et al., 2020) or along strike (Mohn et al. 2015, Ding et al., 2020; Péron-Pinvidic et al., 2017; Lei et al., 2020) of a continental margin. This variability is better expressed in small basins with limited oceanic crust such as in Southeast Asia. Imaging, describing and interpreting in detail the variations of the tectono-sedimentary evolution of a rifted margin covered by a large amount of data, including a new seismic line crossing both conjugate margins, provides crucial opportunities to unravel the tectonic processes and parameters involved in the opening of an ocean (e.g., Abdelmalak et al., 2019; Gernigon et al., 2019; Gillard et al., 2015).

Numerous marginal basins have opened around the Pacific Ocean, for which subduction has influenced the mode of extension and breakup (Taylor and Hayes, 1983). Compared to rift systems in stable continents, rifting close to a subduction zone presents specific characteristics in terms of crustal composition (Persaud et al., 2003; Savva et al., 2014), initial lithospheric thermal structure (Di Luccio et al., 2014; Li et al., 2019) and instability in the orientation of kinematic forces through time (e.g., Western Mediterranean Sea; Van Hinsbergen et al., 2014). Our investigation area, the South China Sea (SCS), is the largest marginal basin of SE Asia and is characterized by a remarkable oceanic V-shaped propagation form Early Oligocene to mid Miocene (Briais et al., 1993). Its tectonic evolution has been extensively studied with a large

variety of geological and geophysical data (Nissen et al., 1995; Cameselle et al., 2015; Larsen et al., 2018; Lei et al., 2018; Li et al., 2015; Liang et al., 2019; Luo et al., 2021) which provide an exceptional dataset for analyzing rifting processes in 3D. However, most of the studies are focused on the SE China margin and a better integration of the tectono-sedimentary evolution along the Xisha Islands-NW Borneo conjugate margins is needed to analyze the spatial and temporal variations of deformation style along and across the SCS.

This paper proposes to investigate the rift evolution of the SW sub-basin of SCS by combining several seismic sections to illustrate both along strike and along dip architectural variations (Fig.1). Our analysis of the extensional structures is focused near a 1000 km long seismic profile (line CFT, Fig.1) crossing the Xisha Islands -NW Borneo conjugated continental margins. To highlight the lateral variations of rifted structures along the margins, we include the interpretation of seismic lines next to the CFT line, which are also crossing the continent-ocean transition (COT) of the conjugate margins (Fig.1). Our analysis is then compared to another segment of the SCS (E sub-basin) (Nirrengarten et al., 2020) which presents tectonic processes resulting in a similar crustal architecture but from an earlier breakup before the propagation of the oceanic system to the southwest. Integrated into the tectono-stratigraphic framework of the SCS margins, this study provides solid arguments to discuss the mode of continental breakup and the extensional process (symmetric or asymmetric architectures, Nirrengarten et al., 2016; Ros et al., 2017 in terms of the rifting mode; depth-dependent extension, Clift et al., 2002; Davis and Kusznir, 2004). The inferred regional stratigraphic correlations provide implications on the influence of the subduction zone on kinematic reorganizations.

2 Geological Background

Extension in the southeast of the South China Block initiated in Late Cretaceous in the tectonic setting of convergence between the Pacific Plate and Eastern Eurasia (Jahn et al., 1976; Sewell and Campbell, 1997; Chan et al., 2010, Nanni et al., 2017, Ye et al., 2018; Zhang et al., 2019). This end of this convergence phase correlates with significant granitic intrusion events south of China. The resulting granitoids have been sampled onshore and offshore by drilling and dredges such as in the Spratly Islands and the Reed Bank area (Kudrass et al., 1986; Yan et al., 2010; Khanchuk et al., 2019; Xiao et al., 2019). The compressional Mesozoic structures such as broad folds flanks or thrust faults were later reactivated by localized normal faults along the granitoids blocks (Savva et al., 2014; Ye et al., 2018). The first cycle of extension took place from the Late Cretaceous to Paleocene with the development of narrow basins filled by coarse-clastic sediments, which evolved into a distributed rifting event in the proximal margins (Teng and Lin, 2004; Yan et al., 2001; Xie et al., 2006; Yao et al., 2012; Steuer et al., 2014). This first extensional event reflects the initial stretching of the continental lithosphere and is observable onshore (Chan et al., 2010; Nanni et al., 2017; Schlutter et al., 1996). The second extensional event (Eocene-Oligocene) corresponds to the main thinning event (Ru and Pigott, 1986; Su et al., 1989; Clift and Lin, 2001; Yan et al., 2001; Ding et al., 2013, Franke et al., 2014; Larsen et al., 2018; Nirrengarten et al., 2020; Cameselle et al., 2020) leading to the propagation of continental breakup from the Early Oligocene to Middle Miocene (Briais et al., 1993; Li et al., 2014a). Most of the rifted basins in the northern (Savva et al., 2013; McIntosh et al., 2014; Gao et al., 2015; Lei and Ren, 2016; Ding et al., 2020) and southern margin of the SCS (Franke et al., 2011; 2014; Ding et al., 2013; Clerc et al., 2018; Peng et al., 2018; Liang et al., 2019) have been shaped during this phase.

Many Cenozoic unconformities have been identified in the conjugate margins of the SCS (Morley, 2016; Lunt, 2019), exhibiting a diachronous opening from east to southwest (Franke

et al., 2014; Chang, 2020; Luo et al., 2021; Pubellier et al., 2021). The identification of those unconformities leads to the definition of a breakup sequence for the SCS margin (Zhao et al., 2016; Alves et al., 2020) which is the sedimentary record during the phase of the diachronic lithospheric breakup (Early Oligocene to Early Miocene). In the SE China margin, the unconformities are associated with a series of normal faults and low-angle detachment faults that accommodated the stretching of the crust (Lei et al., 2019; Xie et al., 2019; Luo et al., 2021). The detachment faults rooted either at the top of ductile layers (lower crust) or at the Moho (Gong et al., 2019; Xie et al., 2019; Deng et al., 2020; Luo et al., 2021). Recently IODP Expedition 367/368 have discovered altered or fresh basalts and pre-rift sedimentary rocks in a narrow distance, representing the oceanic and continental basement lithologies, respectively. These drilling observations significantly constrain the breakup mechanism and the architecture of conjugate margins along the Eastern oceanic sub-basin, disclosing a rapid transition from continental rifting to oceanic spreading within a 10 Myr interval (Larsen et al., 2018; Nirrengarten et al., 2020). The narrow COT in the SCS was independently recognized in the geophysical dataset via various criteria, such as Moho reflection gap, basement morphology and gravity anomaly characteristics (Song et al., 2019, Fig.1b). Some authors proposed an asymmetrical breakup phase in the early times followed by a more symmetrical and stable spreading after 28 Ma (Nirrengarten et al., 2020; Lei et al., 2019).

The conjugate margin in the southwestern SCS is less known because of the thick Eocene to Late Miocene carbonate cover on the NW Borneo margin (Madon et al., 2013; Franke et al., 2011; Steuer et al. 2014; Chang et al., 2015; Jamaludin et al., 2017) and on the Xisha Islands Margin (Fyhn et al., 2013; Vu et al., 2017). These wide rifted margins (> 400 km) are characterized by a relatively flat and shallow Moho (depth 20 km) imaged by refraction data which suggest a weak lower crust in the Xisha Islands Margin (Hayes and Nissen, 2005, Pichot

et al., 2014; Lü et al., 2016; Dong et al., 2018; Huang et al., 2019; Cameselle et al., 2020). There, extensional features, including large detachment faults, accommodated significant thinning of the crust. Some of these structures may result from the reactivation of inherited low-angle thrusts (Savva et al., 2013, Liang et al., 2019). The tectono-magmatic interpretation also reveals a proto-oceanic crust, which corresponds to the incipient onset of seafloor spreading in the southwestern SCS (Luo et al., 2021).

Based on bathymetry and magnetic anomalies (Fig. 1), a change in the spreading direction linked with a ridge jump around 23 Ma has been suggested (Briais et al., 1993; Lee and Lawver, 1995; Barckhausen et al., 2014; Li et al., 2014b; Qiu et al., 2016). Sibuet et al. (2016) and Lei and Ren (2016) have proposed an intermediate spreading event between the two stages around 23Ma. Numerical modelling shows that tectonic loading in the propagation direction may explain a stalling phase of the E-W propagation from 32 to 23 Ma. A change in boundary forces at the regional scale is then likely ending this stalling phase, eventually followed by NE-SW propagation across the whole region from 23 to 16 Ma (Le Pourhiet et al., 2018; Jourdon et al., 2020). However, the exact cause of the change in boundary forces leading to ridge re-orientation is yet unclear.

3 Data Acquisition, Processing and Methods

3.1 Data Acquisition and Processing

We use the China-France Transect MCS profile (CFT) in the vicinity of Penxi Bank and Spratly Islands (Nansha Islands) (Figs.2 and 4). This 1000 km long multichannel seismic (MCS) data was collected by a project conducted by CNRS and Ecole normale supérieure (ENS, France) and Guangzhou Marine Geological Survey (GMGS, PRC), from 2011 to 2013. The vessels, R/V DongFang KanTan and R/V Tan Bao, triggered shots at a 50 meters interval for reflection

profiles after collecting a refraction profile along the transect. The volume of the airgun array was roughly 7,000 cubic inches, and the streamer was 8 kilometers (640 channels) long in the Qiongdongnan area and 6 km (480 channels) along the rest of the profile. Both streamers have a 12.5 meters receiver interval. The record length is 16 sec TWT (seconds two-way travel time) with a 2 ms sampling rate.

This study integrates the results of the whole CFT profile across the conjugate margin of the southwest margin of the South China Sea. The processing was completed at ENS and was designed to enhance the deep crustal structure by several procedures of multiple attenuation. The workflow included geometry, filter, noise attenuation, trace editing, amplitude scaling, bin centering, offset regularization, predictive deconvolution, multiple attenuation (SRME, Radon, and F-K filter), and high-density velocity analysis, all using the CGG Geovation 2013 software. The migration was achieved by pre-stack Kirchhoff time migration, and a dynamic gain (AGC) was applied to the final output image. The high-resolution images are presented in Figure S1 and S2 in the supplementary material.

The efficiency of the anti-multiple procedure varies along the line because of the changes in impedance contrasts of the seafloor and basement. In many areas where the sedimentary package is thin, waves reflected from the basement scatter a lot of energy that is difficult to attenuate (from km 450 to 550 on the CFT-N, and km 150 to 270 on the CFT-S). In addition, two other pieces of seismic profiles, INL320 and NGH-1-3, were acquired and processed by Guangzhou Marine Geological Survey in PRC with a workflow similar to the one already described. The acquisition parameters are shown in the Table.1.

3.2 Interpretation Criteria

For the interpretation, the seismic reflections allow us to distinguish the crust and the sedimentary basins by interpretation of the Moho, basement and sedimentary sequences. Around 9 sec TWT, strong-amplitude reflectors appear intermittently as the Moho surface along the proximal domain. The Moho reflectivity is clearly visible along the north of the CFT line where sedimentary basins are thick, but it is not so obvious in some other sections of the profile. In areas of weak or absent Moho reflectivity, we use results from the refraction velocity models in Pichot et al. (2014) and Liang et al. (2019) to indicate the Moho on our interpretations. These refraction studies use wide angle reflections on the Moho along the coincident refraction line to constrain the Moho depth (with 50 ocean bottom seismometers). More details on how to differentiate the crustal reflectors and the residual multiples along the same seismic line can be found in Liang et al. (2019).

The stratigraphic patterns can be consistently observed along the 1000 km-long seismic line and two shorter lines. The typical syn-rift pattern characterizes the growth strata thickening toward the major normal faults during the rifting stage. In this study, the syn-rift unit has been delimited into two sub-units by an intra-rift unconformity (Fig.2-5). The lower sub-unit, syn-rift I, characterizes strong amplitude reflectors and a wedge-shaped geometry in the proximal margin (orange color on Fig. 2). The upper sub-unit, syn-rift II, overlying the unconformity shows a relatively uniform thickness across the rift basins which only slightly thickens toward depocenters. The intra-rift unconformity (green horizon, IRU) is delimiting two syn-rift packages (I and II) which present an onset of developing the extensional detachment faults (Fig. 2-3). Similar intra-rift unconformities have been recognized in the Pearl River Mouth Basin (Xie et al., 2019). On the top of the syn-rift II, the breakup unconformity (BU) correlate from the other studies (Yao et al., 2012; Savva et al., 2013; Steuer et al., 2014; Lei and Ren, 2016; Vu et al., 2017), characterizing the termination of developing growth strata (Figs. 2 and 3). The

later post-rift unit shows a horizontal to sub-horizontal depositional pattern indicating the rifting has been terminated.

Due to absent of public well data along the seismic profiles in this study, the age for each unit is correlated from the adjacent basins. In the north, Xisha Islands margin based on correlation with seismic profiles tied with wells in adjacent Phu Khanh and Qiongdongnan basins (Vu et al., 2017; Savva et al., 2013; Lei and Ren, 2016), which is identified an unconformity around 32 Ma (T70) and the BU at 23 Ma (T60). In the south, it shares a similar rifting history with the northern margin during the Paleogene (Holloway, 1982; Liang et al., 2019; Bai et al., 2020; Zhang et al., 2020b). The age constraint is established on the base of the well Sampaguita-1 continuously documenting Cenozoic strata and encountering the Mesozoic strata (location S-1 on Figs.1a and 6; Taylor and Hayes, 1980; Yao et al., 2012; Steuer et al., 2014). The result shows two unconformities have been dated in Upper Eocene and Upper Oligocene in the Paleogene strata.

4 Interpretation Results along the CFT Line crossing the Conjugate Margins

To decipher the crustal architecture and extensional processes of the conjugate margins of the SW sub-basin, the long CFT transect is hereafter divided into two parts: the northern section (CFT-N) and the southern section (CFT-S).

4.1 Xisha Islands Margin of the SW sub-basin

The CFT-N profile extends over a 600-kilometer length of thinned crust (from the shelf break to the COT) along the Xisha Islands margin. The crustal thickness varies from 2 to 8 sec TWT (Fig. 2), approximately 6.5 to 25 km thick, showing similarities with the thinned and hyper-thinned domains described in others parts of the SCS (Savva et al., 2013; Lei and Ren, 2016;

234 Cameselle et al., 2020; Nirrengarten et al., 2020). The Moho shallows gently seaward within a
235 few hundreds of kilometers with local fluctuations lower than 1 sec TWT (Fig.2). On the top of
236 the basement, normal faults dip both seaward or landward and bound the edges of the basins
237 with various offsets from 1 to 3 sec TWT at the top of the basement (Fig.3). Large number of
238 normal faults affect the basement with limited throw within 1 sec TWT (grey arrows in distance
239 70 and 250 km on Figs. 3). These structures are mostly associated with the lower syn-rift unit,
240 suggesting an activity during the early stage of rifting, namely syn-rift I in this study. For the
241 larger offset of basement which can reach to 3 sec TWT, the fault bounding the main blocks
242 can be followed roughly until 7-8 sec TWT depth (black arrows in Fig.3), where some
243 horizontal reflectors may be traced to underline a detachment or décollement level (reflector D
244 at distance 70, 220, and 330 km on Fig. 3). The detachment faults rotated the continental block
245 above the lower crust and created accommodation space through most of the syn-rift period
246 (distance 220 km on Fig.3b). However, these detachment reflectors are not obvious in the distal
247 margin because of the strong artifact noise of basement multiple in the CFT-N profile (400 to
248 560 km on Fig.2).
249
250 Within the sedimentary unit, strong amplitude reflectors are traced at the bottom of the
251 Qiongdongnan and Zhongjiannan Basins within 2 sec TWT thickness, approximately 4 km
252 thick (distance 200 to 220 km on Fig.3). The same seismic characteristics are vanishing seaward
253 and are barely observed in the distal part. The syn-rift II is characterized by a slight thickening
254 of the unit toward low angle detachment faults (black arrows on Fig.3), associated with their
255 development. Within syn-rift II, several newly developed faults dipping toward the depocenter
256 offset mainly syn-rift II (Fig.3a and 3b), and terminate at a similar depth as the detachment
257 faults. After the breakup unconformity, the post-rift unit characterizes generally horizontal to
258 sub-horizontal sedimentation under the thermal subsidence. A significant unconformity within

post-rift succession marks the end of extension in the SCS around the Middle Miocene (blue on Fig.3), and has been identified in the southwestern SCS margins (Hutchison, 2004; Hutchison, 2005; Clift et al., 2008; Savva et al., 2013; Vu et al., 2017; Li et al., 2014b). Fluid or gas migration and volcanic bodies can be sporadically found in the post-rift succession shallower than 2 sec TWT (Fig.3). Large amount of delta sediments sourced from the Vietnam coast cover the proximal margin (Fig.3a).

4.2 Northwest Borneo Margin of the SW Sub-basin

The NW Borneo margin rift basins associated with rift basins extends over 600 kilometers southward to Sabah as seen on the seismic and gravity data (Cullen et al., 2010; Bai et al., 2020). The 330 km long seismic profile CFT-S across the NW Borneo Margin illustrates a part of the configuration of the southern margin (Fig. 4). Nevertheless, the crustal structures provide similarities with the northern margin in terms of crustal thickness as well as style of faults. The limited throw faults offset the top of the basement 1 sec TWT (Fig.5c). Detachment faults have been identified underlying a deep basin (reflector D at distance 90 and 30 km on Fig.5b and 5c) as documented in Liang et al. (2019). Several closely-spaced normal faults appear between these detachments (arrows on Fig. 5c).

The lower sedimentary package (syn-rift I) in the proximal domain (distance 0 to 50 km on Fig. 5c) resembles in age with those of the Xisha Islands margin and vanishes seaward (orange color on Fig. 4). Compared to the syn-rift I, the thick sedimentation of syn-rift II reveals major subsidence prior to the breakup at distance 70 km (Figs. 5b and 5c). The syn-rift II unit thickens toward low-angle detachment faults and is also offset by several newly developed faults (arrows on Fig.5c). A post-rift erosional surface (blue horizon) overlies the lower post-rift sediments and part of the syn-rift succession (distance 30 km on Fig.5c) with significant P-wave velocity

284 contrast (approximately from 1.6 km/s to 3.8 km/s or 2.9 km/s to 5.3 km/s estimated by Wang
285 et al., 2016). Many post-rift volcanic rocks are observed along the profile (Figs. 4 and 5a) and
286 the adjacent area in the NW Borneo Margin (Chang et al., 2017; Zhang et al., 2020b).
287
288 **5 Interpretation results along two profiles crossing the Continent-Ocean Transition**
289 Around the previously described CFT line, the rifted margin displays lateral structural
290 variations along the COT of the Southwest SCS. An abrupt bathymetric contrast marks an N-S
291 lineament at the eastern edge of the Penxi Bank and the western edge of the Spratly Islands
292 crustal morpho-structures (Fig.6a). In contrast, a gradual slope characterizes an E-W morpho-
293 structure at the south of the Penxi Bank (Fig.6a). Two extracted profiles illustrate the crustal
294 architecture of the N-S segment (Fig.7a and 7b) and the E-W segment (Fig.9a and 9b). We
295 completed the observation by interpreting two other pieces of seismic profiles, namely INL320
296 and NGH-1-3 (Fig.9a and 9b).
297
298 We have reconstructed the conjugated margin on a cross-section (Fig.7 and 9) at C5En (18.8
299 Ma, Briais et al., 1993, which is the similar age in Li et al., 2014a) (Fig.6b) by removing the
300 oceanic crust. This study extrapolates the magnetic anomalies along the bathymetric features
301 and suggests ages for the formation of the oceanic crust in areas where the magnetic anomalies
302 are blurred southwestward (Fig.6b). Interestingly, the magnetic modelling along profiles
303 defined the earliest anomaly at C6n (20.1 Ma) on southern side and at C5En (18.8 Ma) on the
304 northern side (Fig.6b).
305
306 **5.1 N-S Trending Segments of the Margin**
307 The thickness of the crust, tracked by intermittent Moho reflectors, thins oceanward from a
308 depth of 10 sec to 8 sec TWT (Fig.7). This reflector runs beneath the continental basement

around 10 sec TWT in the NW Borneo margin, and ascends seaward adjacent to the oceanic crust near the magnetic anomaly C6n (Fig.8b). The extension at the edge of the basin (black arrows on Fig.7a) may reach a possible level of detachment fringing the lower crust, although the base reflector is not as clear as the detachment level seen in the landward basins. Next to the magnetic anomalies, the basement slope at the COT area steepens along the E Vietnam margin than at the conjugate NW Borneo margin, displaying an asymmetric structure (Fig.7).

The overlying syn-rift II sediments are restricted to small depressions, which displays a relatively thin sedimentary infill. Stratigraphy may record a hiatus (breakup unconformity) indicated by significant erosional surfaces from basin to basement on both margins (red horizon on Fig.8a). It indicates that the crust did not undergo significant subsidence during the rifting and was sustained at shallow water depth before breakup (Liang et al., 2019). Some chaotic facies at the bottom sedimentary succession probably resulted from mass transport deposits along the abrupt slope adjacent to the COT (Fig. 8b).

5.2 E-W Trending Segments of the Margins

By contrast, the E-W trending segments display a thinner crust with a large amount of sediments near the COT (Fig.9). The asymmetrical architecture of the crust is shown by the thinner crust and lower basement slope in the south. The basement is offset by northward-dipping faults in the NW Borneo Margin whereas the top of the basement is rather smooth in the E Vietnam Margin (Fig.10b and Fig.10c). Part of the basement with magmatic addition is barely covered by syn-rift succession and no significant Moho reflector is observed, adjacent to the location of the first magnetic anomaly in the NW Borneo Margin (Figs.9b and 10c). Such a configuration may perhaps indicate an exhumation of sub-continental lithospheric mantle (Ding et al., 2016) or part of the lower continental crust. The syn-breakup volcanic additions are also revealed, for

instance, intruded magmatic bodies in the NW Borneo Margin and a high-amplitude reflector beneath the Moho in the E Vietnam Margin (Figs. 10b and 11c).

The horizon at the top of the syn-rift II correlates to the top of the basement in the oceanic domain and, therefore, is interpreted as a period occurring the continental breakup (Figs. 9-10). The correlation of the top of the syn-rift II may be extended landward (red horizon on Figs. 9a and 10a). The underlain syn-rift II is characterized by a relatively uniform thickness (slightly thicker toward the oceanic crust), and a total width of both margins reaches 75 km in length (Figs. 10b and 10c). A series of dense normal faults mildly offset most of the syn-rift succession and dip seaward in both conjugated margins (Fig.10), which is consistent with the observation of syn-rift II in the proximal margins. This syn-rift II has concave-up disturbance and truncation atop localized at the seaward boundary of the COT. The post-breakup unit onlapped the unconformity, also interpreted as breakup sequence in the SCS (Lei et al., 2019; Alves et al., 2020; Zhang et al., 2020b). The oceanic domain and the COT are overlain unconformably by post-rift strata.

5.3 Lateral Variation of the COT Structures

In the Southwest SCS, the crustal architecture appears to differ depending on the orientation of the COT. We have observed a significant variation of sediment thickness and a sharp difference between the N-S and the E-W margin segments (crossed by obliquely oriented seismic profiles, Figs.11b and 11c). At the COT, the E-W segment illustrates more hyper-extended crust and more sediment infill (Fig. 11c). Instead, segments connected by N-S abrupt relays exhibit a sharp COT with thin overlying sediments (Fig. 11d).

6. Discussion

6.1 Margin Configuration prior to the Continental Breakup

The observation of the two sections in the southwest of the SCS allows us to compare the extensional and magmatic processes at the termination of the continental crust (COT) with the margins of the eastern SCS (Fig. 11a). Being juxtaposed, the margins show a similar hyper-extensional aspect in the profiles crossing the E-W margin segment (Fig.11c). The conjugate profile selected for the East sub-basin (Nirrengarten et al., 2020, Fig 11a) and the Southwest sub-basin (this study Fig. 11c) of the SCS show an asymmetrical architecture presenting a respectively southward- and northward-dipping detachment fault. In fact, the orientation and separation of the faults in the distal domain on the two conjugate margins allow us to retrieve the tectonic evolution of an extensional wedge to determine the direction of the basal shear (Xiao et al., 1991). Indeed, following the morphological criterion examine by Nirrengarten et al. (2016), the SE China and the NW Borneo are defined as lower plate margins architecture. Moreover, in terms of magnetic anomaly, it appears that both systems display their oldest marine magnetic anomaly on the lower plate side, whereas it is absent from the conjugate side (C11n and C6n on Fig. 11). This has been suggested to be related to an initial asymmetrical spreading of the SCS ridge (Nirrengarten et al., 2020). In the distal margin morphology and on the oldest oceanic crust the structures and magnetic properties of the conjugate margins of the SW and E sub-basin are similar and seem to involve similar tectonic and magmatic processes during the break-up.

We have restored the position of the Spratly Islands (Nansha Islands) and Penxi Bank around breakup time using the magnetic anomaly from Briais et al, (1993) (Fig.12). The obtained map presents basins with rhomboid shape, which is composed of a chain of “en echelon” basins stretching in an N-S direction near the COT (Fig.12). Their geometry demonstrates E-W hyper-extended basin terminated by N-S strike-slip faults. The syn-rift strata are mainly deposited in

an E-W orientated basin along the gradual slope in bathymetry, suggesting a thinning in agreement with N-S extension. The N-S segments, on the contrary, would have suffered a relative wrench component, thus making the early COT system compatible with the sediment-starved segment.

These are compatible with a right-lateral motion between the Vietnam Fault (Marquis et al., 1997; Roques et al., 1997; Fyhn et al., 2009) and the Zhongnan Fault (Li et al., 2015) (Fig.12). Along the N-S segment, no clear strike-slip and transtensional structures are observed on the seismic profiles but have been observed from potential-field data (Hwang and Chang, 2014). The lateral variation of syn-rift thickness deciphers the former basin architecture in this study. We suggest that the connection of the isolated basins produces a stress release which induces a rapid propagation of breakup into the continental margin toward the southwest. This propagation of the deformation has been proposed for the incipient breakup of the Red Sea (Augustin et al., 2014; Ligi et al., 2018) highlighted by the node model described in Zwaan et al. (2020) or oblique rifting described in Jourdon et al. (2020).

However, the later seafloor spreading in NW-SE direction forms an angle of 30° with these pull-apart basins. It has been accepted that seafloor spreading changed progressively into NW-SE direction based on the magnetic and bathymetry analysis (Briais et al., 1993; Sibuet et al., 2016; Lee and Lawver, 1995). As a result, not only the direction of seafloor spreading recorded the shift; the adjacent rifted basins also display changes in the direction of opening and the amount of sediments deposited. We suggest that the N-S rifting in the southwestern SCS was compatible in orientation with the first phase of seafloor spreading in N-S direction from 32 to 23 Ma (Briais et al., 2013; Barckhausen et al., 2014). It was followed by an “intermediate” period around the ridge jump accommodated by the N165° extensional direction, proposed by

Sibuet et al., (2016). A similar change of extensional direction is also shown in the Phu Khanh Basin after the Middle Miocene (Savva et al., 2013). Numerical simulation suggests that oceanic propagation was stalled at the boundary between the eastern and southwestern basins because of far-field compression in the EW direction (Le Pourhiet et al., 2018). The far-field stress direction necessarily had to change to resume and shift propagation toward the southwest.

6.2 Break-up Evolution in the SW Margin

The tectono-stratigraphic analysis offers a scenario for the break-up evolution in the Southwest SCS. The detachment faults play an important role in the thinning of the SCS continental crust and in exhumation of the lower crust or the lithospheric mantle, preserving an asymmetrical structure (Fig.13c). The deposition of the syn-rift II is associated with the development of detachment faults, subsequently offset by seaward-dipping normal faults during the latest rifting stage. A ductile layer is probably required underneath the detachment fault to accommodate the subsidence at the depocenter (Fig.13b) as interpreted previously in adjacent Qiongdongnan Basins and Xisha Trough (Clift et al., 2002; Davis and Kusznir, 2004; Pichot et al. 2014, Lei and Ren, 2016; Xie et al., 2019; Lei et al., 2019; Bai et al., 2020). This could favor the depth-dependent decoupling as suggested in several simulations in the case of wide rifted margins (Huismans and Beaumont, 2011; Clift and Lin, 2001, Brune et al., 2017; Ros et al., 2017).

The tectono-stratigraphy of the syn-rift II has been discussed in several papers with varying interpretations for pre-rift, syn-rift and post-rift, of the COT area, due to a lack of well-established bio-stratigraphy studies (Ding et al., 2013; 2016; Song and Li, 2015; Wang et al., 2016; Luo et al., 2021). However, the sedimentary package underneath the red horizon (20Ma, Early Miocene) can be confidently traced with similar seismic facies and mild-offset normal

faults on both margins vanishing toward the oceanic domain and is therefore considered as syn-rift. (Fig. 10b and 10c). The significant unconformity (blue), which tops the unit offset by the small normal fault, is considered as Late Miocene based on correlation from the biostratigraphy of the IODP Site U1433 (Li et al., 2015).

The similarity of structural evolution enables us to propose that the U-shaped seismic facies of syn-rift II (Lower Oligocene) in the East SCS may be also related to the similar development of detachment faults (Fig.11a). The margins of the Southwest Sub-Basin experienced a longer period of extension than margins of the East Sub-Basin, and hence resulted in thinner crust in several basins, for instance, the Qiongdongnan Basin (Fig.2) and basins near the COT (Fig.11), for which the crustal thickness reaches values thinner than 1.5 sec TWT. In several adjacent basins, we can barely observe relics of crust at the depocenter, such as in the Phu Khanh Basin and the Nam Con Son Basin (Savva et al., 2013; Lei and Ren, 2016; Clerc et al., 2018; Lei et al., 2020). This period of the syn-rift II corresponds to mostly horizontal motion on low angle detachment faults, varying in time as the breakup propagated toward southwest. (R2 unit in Fig.14).

The continental lithosphere was finally broken up by the ascending asthenosphere which produced volcanic edifices as well as magmatic intrusion within the crust (Fig.13b). The syn-rift II succession adjacent to the COT with concave-up features implying an uplifting movement possibly during oceanic crust formation (Fig.10b and 10c), and was therefore accompanied by an unconformity on top. The later sequence as post-breakup shows the subsequent subsidence after the lithospheric breakup, and described as the onset of deposition of breakup sequence in Zhang et al. (2020b). The forced deformation of the syn-rift II is associated with the underneath magmatic additions as well as subsequent seafloor spreading after the deposition of syn-rift II,

favoring the tectono-magmatic process in a narrow time span (Fig. 13b) rather than concurrent with the depositing syn-rift units (unit T3 in Luo et al., 2021). The lithospheric breakup was immediately followed by creating asymmetrically an extrusive volcano with the cone shape and a first magnetic anomaly C6n in the south (Fig.11b and 11c). The narrow COT infers a rapid process in which the propagator leads to the lithospheric breakup in the southwest SCS, as proposed by recent studies (Cameselle et al., 2020).

6.3 Impact of the Subduction South of the SCS

On the seismic profile, a Miocene erosional event on Fig. 5c extends toward the accretionary wedge of the PSCS subduction in the Palawan and Borneo area (Steuer et al., 2014; Ding et al., 2015; Tong et al., 2019). As the tectono-stratigraphy of the SCS and the Borneo-Palawan area, a correlation of the seafloor spreading shift in the South China Sea and the Borneo-Palawan orogeny highlights a time around 23Ma (Top Crocker Unconformity, TCU on Fig. 14; Cullen, 2010; Lunt et al., 2019). The propagator continued advancing southwestward subsequently until the extensional stress died out around 16 Ma as well as the termination of orogeny in Sabah (Chang et al., 2019) (Fig. 14). The change of direction of seafloor spreading is also concurrent with the rotational movement of the northern Borneo and Palawan as deduced from paleomagnetic analysis, which shows a counter-clockwise rotation during Early Miocene (Fuller et al., 1999; Cullen, 2010; Advokaat et al., 2018). Therefore, we suggest that the orogeny-related tectonic in Borneo may have modified the direction of opening from N-S to NW-SE by changing the far-field stress in the South China Sea.

7. Conclusion

This study has explored the crustal architecture and evolution of the southwestern South China Sea. The 1000 kilometer long profile illustrates distributed rifted basins, which thinned owing

484 to low-angle detachment faults rooted into the top of ductile layers in the lower level of the
485 continental crust. The continental lithosphere stretching and thinning are accommodated by
486 ubiquitous large detachments in the Xisha Islands-NW Borneo margins. Tectono-stratigraphic
487 analysis in the vicinity of the COT suggests that hyper-extension is restricted to the E-W
488 segments of the distal margin, whereas the N-S segments are abrupt and covered by a thin
489 blanket of sediments overlying the basement. The conjugate E-W segment presents an
490 asymmetric distal margin with a well-defined lower plate structure on the NW Borneo margin
491 similar to the one observed on the SE China margin bordering the eastern SCS. These COT
492 boundaries delineate small "en echelon" rifted basins whose distribution is indicative of a right-
493 lateral motion prior to 23 Ma, during the first phase of seafloor spreading in the East SCS. Most
494 of the extension developed in the N-S direction prior to breakup, and then started to change
495 progressively to the NW-SE during the second phase of spreading. The pull-apart basins would
496 thus underline the transitional period. In that sense, the succession of events is strikingly coeval
497 to the far-field stress change induced from the adjacent subduction and closure of the Proto-
498 South China Sea in Palawan-Borneo.
499
500 **Acknowledgement**
501 This work is the result of a long-lasting cooperation, initiated in 2008, between ENS-PSL /
502 CNRS in Paris, France, and Guangzhou Marine Geological Survey (GMGS), in China. Ship
503 and seismic equipment were supplied by GMGS. MCS data processing had been performed at
504 ENS. We thank CGG for giving us access to the CGG Geovation 2013 software. The raw
505 seismic data set can be found online (www.geologie.ens.fr/imagerie/). We are also grateful for
506 the useful suggestions of S. Steuer, anonymous reviewers and the editor Dr Tiego Alves.

507 **References**

508 Abdelmalak, M.M., Planke, S., Polteau, S., Hartz, E.H., Faleide, J.I., Tegner, C., Jerram, D.A.,
509 Millett, J.M., Myklebust, R., 2019. Breakup volcanism and plate tectonics in the NW
510 Atlantic. Tectonophysics 760, 267–296.

511 Advokaat, E. L., Marshall, N. T., Li, S., Spakman, W., Krijgsman, W., and van Hinsbergen, D.
512 J. J., 2018, Cenozoic Rotation History of Borneo and Sundaland, SE Asia Revealed by
513 Paleomagnetism, Seismic Tomography, and Kinematic Reconstruction: Tectonics, v. 37, no.
514 8, p. 2486-2512.

515 Alves, T. M., Fetter, M., Busby, C., Gontijo, R., Cunha, T. A., and Mattos, N. H., 2020, A
516 tectono-stratigraphic review of continental breakup on intraplate continental margins and its
517 impact on resultant hydrocarbon systems: Marine and Petroleum Geology, p. 104341.

518 Augustin, N., et al. (2014). "The rifting to spreading transition in the Red Sea." Earth and
519 Planetary Science Letters 395: 217-230.

520 Bai, Y., Wang, X., Dong, D., Brune, S., Wu, S., and Wang, Z., 2020, Symmetry of the South
521 China Sea conjugate margins in a rifting, drifting and collision context: Marine and
522 Petroleum Geology, v. 117.

523 Barckhausen, U., Engels, M., Franke, D., Ladage, S., and Pubellier, M., 2014, Evolution of the
524 South China Sea: Revised ages for breakup and seafloor spreading: Marine and Petroleum
525 Geology, v. 58, Part B, no. 0, p. 599-611.

526 Briais, A., Patriat, P., and Tapponnier, P., 1993, Updated interpretation of magnetic anomalies
527 and seafloor spreading stages in the south China Sea: Implications for the Tertiary tectonics
528 of Southeast Asia: Journal of Geophysical Research: Solid Earth, v. 98, no. B4, p. 6299-
529 6328.

530 Brune, S., Heine, C., Clift, P. D., and Pérez-Gussinyé, M., 2017, Rifted margin architecture and
531 crustal rheology: Reviewing Iberia-Newfoundland, Central South Atlantic, and South China
532 Sea: Marine and Petroleum Geology, v. 79, p. 257-281.
533 Cameselle, A. L., Ranero, C. R., Franke, D., and Barckhausen, U., 2015, The continent-ocean
534 transition on the northwestern South China Sea: Basin Research, v. 29, p. 73-95.
535 Cameselle, A. L., Ranero, C. R., and Barckhausen, U., 2020, Understanding the 3D Formation
536 of a Wide Rift: The Central South China Sea Rift System: Tectonics, v. 39, no. 12.
537 Chan, L. S., Shen, W., and Pubellier, M. 2010. Polyphase rifting of greater Pearl River delta
538 region south china: Evidence for possible rapid changes in regional stress configuration.
539 Journal of Structural Geology, 32, 746–754.
540 Chang, J.-H., Hsu, H.-H., Liu, C.-S., Lee, T.-Y., Chiu, S.-D., Su, C.-C., Ma, Y.-F., Chiu, Y.-H.,
541 Hung, H.-T., Lin, Y.-C., and Chiu, C.-H., 2015, Seismic sequence stratigraphic analysis of
542 the carbonate platform, north offshore Taiping Island, Dangerous Grounds, South China Sea:
543 Tectonophysics.
544 Chang, S.-P., Fathiyah Jamaludin, S. N., Pubellier, M., Zainuddin, N. M., and Choong, C.-M.,
545 2019, Collision, mélange and circular basins in north Borneo: a genetic link?: Journal of
546 Asian Earth Sciences.
547 Chang. 2020, Impact of the Surrounding Subduction Zones on the Tectonic Evolution of the
548 South China Sea. PhD dissertation. PSL University, Paris
549 Clerc, C., Ringenbach, J.-C., Jolivet, L., and Ballard, J.-F., 2018, Rifted margins: Ductile
550 deformation, boudinage, continentward-dipping normal faults and the role of the weak lower
551 crust: Gondwana Research, v. 53, p. 20-40.
552 Clift, P., and Lin, J., 2001, Preferential mantle lithospheric extension under the South China
553 margin: Marine and Petroleum Geology, v. 18, no. 8, p. 929-945.

554 Clift, P., Lin, J., and Barckhausen, U., 2002, Evidence of low flexural rigidity and low viscosity
555 lower continental crust during continental break-up in the South China Sea: Marine and
556 Petroleum Geology, v. 19, no. 8, p. 951-970.
557 Clift, P.D., Lee, G.H., Nguyen, A.D., Barckhausen, U., Hoang, V.L., Sun, Z., 2008. Seismic
558 evidence for a Dangerous Grounds mini-plate: No extrusion origin for the South China Sea.
559 Tectonics, 27(TC3008). doi:10.1029/2007TC002216.
560 Cullen, A., Reemst, P., Henstra, G., Gozzard, S., and Ray, A., 2010, Rifting of the South China
561 Sea: new perspectives: Petroleum Geoscience, v. 16, no. 3, p. 273-282.
562 Cullen, A. B., 2010, Transverse segmentation of the Baram-Balabac Basin, NW Borneo:
563 refining the model of Borneo's tectonic evolution: Petroleum Geoscience, v. 16, no. 1, p. 3-
564 29.
565 Davis, M. & Kusznir, N. (2004). 4. Depth-Dependent Lithospheric Stretching at Rifted
566 Continental Margins. In G. Karner, B. Taylor, N. Driscoll & D. Kohlstedt (Ed.), *Rheology*
567 *and Deformation of the Lithosphere at Continental Margins* (pp. 92-137). New York
568 Chichester, West Sussex: Columbia University Press. https://doi.org/10.7312/karn12738-
569 005
570 Deng, H., Ren, J., Pang, X., Rey, P. F., McClay, K. R., Watkinson, I. M., Zheng, J., and Luo,
571 P., 2020, South China Sea documents the transition from wide continental rift to continental
572 break up: Nat Commun, v. 11, no. 1, p. 4583.
573 Di Luccio, F., Persaud, P., and Clayton, R. W., 2014, Seismic structure beneath the Gulf of
574 California: a contribution from group velocity measurements: Geophysical Journal
575 International, v. 199, no. 3, p. 1861-1877.
576 Ding, W., Franke, D., Li, J., and Steuer, S., 2013, Seismic stratigraphy and tectonic structure
577 from a composite multi-channel seismic profile across the entire Dangerous Grounds, South
578 China Sea: Tectonophysics, v. 582, p. 162-176.

579 Ding, W., Li, J., Dong, C., and Fang, Y., 2015, Oligocene–Miocene carbonates in the Reed
580 Bank area, South China Sea, and their tectono-sedimentary evolution: Marine Geophysical
581 Research, v. 36, no. 2-3, p. 149-165.
582 Ding, W., Li, J., and Clift, P. D., 2016, Spreading dynamics and sedimentary process of the
583 Southwest Sub-basin, South China Sea: Constraints from multi-channel seismic data and
584 IODP Expedition 349: Journal of Asian Earth Sciences, v. 115, p. 97-113.
585 Ding, W., Sun, Z., Mohn, G., Nirrengarten, M., Tugend, J., Manatschal, G., and Li, J., 2020,
586 Lateral evolution of the rift-to-drift transition in the South China Sea: Evidence from multi-
587 channel seismic data and IODP Expeditions 367&368 drilling results: Earth and Planetary
588 Science Letters, v. 531, p. 115932.Dong, M., Wu, S., Zhang, J., Xu, X., Gao, J., and Song,
589 T., 2018, Lithospheric structure of the Southwest South China Sea: implications for rifting
590 and extension: International Geology Review, p. 1-14.
591 Dong, M., Wu, S., Zhang, J., Xu, X., Gao, J., and Song, T., 2018, Lithospheric structure of the
592 Southwest South China Sea: implications for rifting and extension: International Geology
593 Review, p. 1-14.
594 Franke, D., Barckhausen, U., Baristeas, N., Engels, M., Ladage, S., Lutz, R., Montano, J.,
595 Pellejera, N., Ramos, E. G., and Schnabel, M., 2011, The continent-ocean transition at the
596 southeastern margin of the South China Sea: Marine and Petroleum Geology, v. 28, no. 6, p.
597 1187-1204.
598 Franke, D., Savva, D., Pubellier, M., Steuer, S., Mouly, B., Auxietre, J.-L., Meresse, F., and
599 Chamot-Rooke, N., 2014, The final rifting evolution in the South China Sea: Marine and
600 Petroleum Geology, v. 58, p. 704-720.
601 Fuller, M., Ali, J. R., Moss, S. J., Frost, G. M., Richter, B., and Mahfi, A., 1999,
602 Paleomagnetism of Borneo: Journal of Asian Earth Sciences, v. 17, no. 1-2, p. 3-24.

603 Fyhn, M. B. W., Boldreel, L. O., and Nielsen, L. H., 2009, Geological development of the
604 Central and South Vietnamese margin: Implications for the establishment of the South China
605 Sea, Indochinese escape tectonics and Cenozoic volcanism: Tectonophysics, v. 478, no. 3,
606 p. 184-214.
607 Fyhn, M. B. W., Boldreel, L. O., Nielsen, L. H., Giang, T. C., Nga, L. H., Hong, N. T. M.,
608 Nguyen, N. D., and Abatzis, I., 2013, Carbonate platform growth and demise offshore
609 Central Vietnam: Effects of Early Miocene transgression and subsequent onshore uplift:
610 Journal of Asian Earth Sciences, v. 76, p. 152-168.
611 Gao, J., Wu, S., McIntosh, K., Mi, L., Yao, B., Chen, Z., and Jia, L., 2015, The continent–ocean
612 transition at the mid-northern margin of the South China Sea: Tectonophysics, v. 654, p. 1-
613 19.
614 Gao, J., Bangs, N., Wu, S., Cai, G., Han, S., Ma, B., Wang, J., Xie, Y., Huang, W., Dong, D.,
615 and Wang, D., 2019, Post-seafloor spreading magmatism and associated magmatic
616 hydrothermal systems in the Xisha uplift region, northwestern South China Sea: Basin
617 Research.
618 Gee, J. S., and D. V. Kent (2007), Source of oceanic magnetic anomalies and the geomagnetic
619 polarity time scale, in Treatise on Geophysics, vol. 5, chap. 12, edited by M. Kono, pp. 455–
620 507, Elsevier, Amsterdam.
621 Geng, M., Song, H., Guan, Y., Chen, J., Zhang, R., Zhang, B., and Zhang, X., 2020, Sill-related
622 seafloor domes in the Zhongjiannan Basin, western South China Sea: Marine and Petroleum
623 Geology, v. 122.
624 Geological Survey of Japan and Coordinating Committee for Coastal and Offshore Geoscience
625 Programmes in East and Southeast Asia (CCOP). (1996). Magnetic anomaly map of East
626 Asia 1:4,000,000 CD-ROMVersion, Digital Geoscience Map 2 (P-1).

627 Gernigon, L., Franke, D., Geoffroy, L., Schiffer, C., Foulger, G.R., Stoker, M., 2019. Crustal
628 fragmentation, magmatism, and the diachronous opening of the Norwegian-Greenland Sea.
629 Earth-Science Rev.
630 Gillard, M., Autin, J., Manatschal, G., Sauter, D., Munschy, M., and Schaming, M., 2015,
631 Tectonomagmatic evolution of the final stages of rifting along the deep conjugate
632 Australian-Antarctic magma-poor rifted margins: Constraints from seismic observations:
633 Tectonics, v. 34, no. 4, p. 753-783.
634 Gong, Y., Lin, C., Zhang, Z., Zhang, B., Shu, L., Feng, X., Hong, F., Xing, Z., Liu, H., and Su,
635 E., 2019, Breakup unconformities at the end of the early Oligocene in the Pearl River Mouth
636 Basin, South China Sea: significance for the evolution of basin dynamics and tectonic
637 geography during rift–drift transition: Marine Geophysical Research.
638 Hayes, D. E., and Nissen, S. S., 2005, The South China sea margins: Implications for rifting
639 contrasts: Earth and Planetary Science Letters, v. 237, no. 3-4, p. 601-616.
640 Holloway, N. H., 1982, North Palawan Block, Philippines - Its Relation to Asian Mainland and
641 Role in Evolution of South China Sea: Aapg Bulletin-American Association of Petroleum
642 Geologists, v. 66, no. 9, p. 1355-1383.
643 Huang, H., Qiu, X., Pichot, T., Klingelhoefer, F., Zhao, M., Wang, P., and Hao, T., 2019,
644 Seismic structure of the northwestern margin of the South China Sea: implication for
645 asymmetric continental extension: Geophysical Journal International, v. 218, no. 2, p. 1246-
646 1261.
647 Hutchison, C. S., 2004, Marginal basin evolution: the southern South China Sea: Marine and
648 Petroleum Geology, v. 21, no. 9, p. 1129-1148.
649 Hutchison, C.S., 2005. Geology of North-West Borneo: Sarawak, Brunei and Sabah. Elsevier,
650 Amsterdam, p 448: 044455890X.

651 Huismans, R., and Beaumont, C., 2011, Depth-dependent extension, two-stage breakup and
652 cratonic underplating at rifted margins: Nature, v. 473, no. 7345, p. 74-78.
653 Hwang, C., and Chang, E. T., 2014, Geophysics. Seafloor secrets revealed: Science, v. 346, no.
654 6205, p. 32-33.Jahn, B., Chen, P.Y., Yen, T.P., 1976. Rb-Sr ages of granitic rocks from
655 southeastern China and their tectonic significance. Geological Society of America Bulletin,
656 87: 763-776.
657 Jamaludin, S. N. F., Pubellier, M., and Menier, D., 2017, Structural Restoration of Carbonate
658 Platform in the Southern Part of Central Luconia, Malaysia: Journal of Earth Science, v. 29,
659 no. 1, p. 155-168.
660 Jourdon, A., Le Pourhiet, L., Mouthereau, F., and May, D., 2020, Modes of Propagation of
661 Continental Breakup and Associated Oblique Rift Structures: Journal of Geophysical
662 Research: Solid Earth, v. 125, no. 9.
663 Khanchuk, A. I., Grebennikov, A. V., and Ivanov, V. V., 2019, Albian–Cenomanian Orogenic
664 Belt and Igneous Province of Pacific Asia: Russian Journal of Pacific Geology, v. 13, no. 3,
665 p. 187-219.
666 Kudrass, H. R., Wiedicke, M., Cepek, P., Kreuzer, H., and Müller, P., 1986, Mesozoic and
667 Cainozoic rocks dredged from the South China Sea (Reed Bank area) and Sulu Sea and their
668 significance for plate-tectonic reconstructions: Marine and Petroleum Geology, v. 3, no. 1,
669 p. 19-30.
670 Larsen, H. C., Mohn, G., Nirrengarten, M., Sun, Z., Stock, J., Jian, Z., Klaus, A., Alvarez-
671 Zarikian, C. A., Boaga, J., Bowden, S. A., Briais, A., Chen, Y., Cukur, D., Dadd, K., Ding,
672 W., Dorais, M., Ferré, E. C., Ferreira, F., Furusawa, A., Gewecke, A., Hinojosa, J., Höfig,
673 T. W., Hsiung, K. H., Huang, B., Huang, E., Huang, X. L., Jiang, S., Jin, H., Johnson, B. G.,
674 Kurzawski, R. M., Lei, C., Li, B., Li, L., Li, Y., Lin, J., Liu, C., Liu, C., Liu, Z., Luna, A. J.,
675 Lupi, C., McCarthy, A., Ningthoujam, L., Osono, N., Peate, D. W., Persaud, P., Qiu, N.,

676 Robinson, C., Satolli, S., Sauermilch, I., Schindlbeck, J. C., Skinner, S., Straub, S., Su, X.,
677 Su, C., Tian, L., van der Zwan, F. M., Wan, S., Wu, H., Xiang, R., Yadav, R., Yi, L., Yu, P.
678 S., Zhang, C., Zhang, J., Zhang, Y., Zhao, N., Zhong, G., and Zhong, L., 2018, Rapid
679 transition from continental breakup to igneous oceanic crust in the South China Sea: Nature
680 Geoscience, v. 11, no. 10, p. 782-789.
681 Le Pourhiet, L., Chamot-Rooke, N., Delescluse, M., May, D. A., Watremez, L., and Pubellier,
682 M., 2018, Continental break-up of the South China Sea stalled by far-field compression:
683 Nature Geoscience, v. 11, no. 8, p. 605-609.
684 Lee, T.-Y., and Lawver, L. A., 1995, Cenozoic plate reconstruction of Southeast Asia:
685 Tectonophysics, v. 251, no. 1-4, p. 85-138.
686 Lei, C., and Ren, J. Y., 2016, Hyper-extended rift systems in the Xisha Trough, northwestern
687 South China Sea: Implications for extreme crustal thinning ahead of a propagating ocean:
688 Marine and Petroleum Geology, v. 77, p. 846-864.
689 Lei, C., Alves, T. M., Ren, J., Pang, X., Yang, L., and Liu, J., 2019, Depositional architecture
690 and structural evolution of a region immediately inboard of the locus of continental breakup
691 (Liwan Sub-basin, South China Sea): GSA Bulletin, v. 131, no. 7-8, p. 1059-1074.
692 Lei, C., Ren, J., Pang, X., Chao, P., and Han, X., 2018, Continental rifting and sediment infill
693 in the distal part of the northern South China Sea in the Western Pacific region: Challenge
694 on the present-day models for the passive margins: Marine and Petroleum Geology, v. 93, p.
695 166-181.
696 Lei, C., Alves, T. M., Ren, J., & Tong, C. (2020). Rift structure and sediment infill of
697 hyperextended continental crust: Insights from 3D seismic and well data (Xisha Trough,
698 South China Sea). Journal of Geophysical Research: Solid Earth, 125, e2019JB018610.
699 https://doi.org/10.1029/2019JB018610

Li, C.-F., Xu, X., Lin, J., Sun, Z., Zhu, J., Yao, Y., Zhao, X., Liu, Q., Kulhanek, D. K., Wang, J., Song, T., Zhao, J., Qiu, N., Guan, Y., Zhou, Z., Williams, T., Bao, R., Briais, A., Brown, E. A., Chen, Y., Clift, P. D., Colwell, F. S., Dadd, K. A., Ding, W., Almeida, I. H., Huang, X.-L., Hyun, S., Jiang, T., Koppers, A. A. P., Li, Q., Liu, C., Liu, Z., Nagai, R. H., Peleo-Alampay, A., Su, X., Tejada, M. L. G., Trinh, H. S., Yeh, Y.-C., Zhang, C., Zhang, F., and Zhang, G.-L., 2014a, Ages and magnetic structures of the South China Sea constrained by deep tow magnetic surveys and IODP Expedition 349: Geochemistry, Geophysics, Geosystems, v. 15, no. 12, p. 4958-4983.

Li, C. F., Li, J. B., Ding, W. W., Franke, D., Yao, Y. J., Shi, H. S., Pang, X., Cao, Y., Lin, J., Kulhanek, D. K., Williams, T., Bao, R., Briais, A., Brown, E. A., Chen, Y. F., Clift, P. D., Colwell, F. S., Dadd, K. A., Hernandez-Almeida, I., Huang, X. L., Hyun, S., Jiang, T., Koppers, A. A. P., Li, Q. Y., Liu, C. L., Liu, Q. S., Liu, Z. F., Nagai, R. H., Peleo-Alampay, A., Su, X., Sun, Z., Tejada, M. L. G., Trinh, H. S., Yeh, Y. C., Zhang, C. L., Zhang, F., Zhang, G. L., and Zhao, X. X., 2015, Seismic stratigraphy of the central South China Sea basin and implications for neotectonics: Journal of Geophysical Research-Solid Earth, v. 120, no. 3, p. 1377-1399.

Li, F., Sun, Z., Pang, X., Liao, J., Yang, H., Xie, H., Zhuo, H., and Zhao, Z., 2019, Low-viscosity crustal layer controls the crustal architecture and thermal distribution at hyper-extended margins: Modeling insight and application to the northern South China Sea margin: Geochemistry, Geophysics, Geosystems, v. 20, no. 7, p. 3248-3267.

Li, L., Clift, P. D., Stephenson, R., and Nguyen, H. T., 2014b, Non-uniform hyper-extension in advance of seafloor spreading on the vietnam continental margin and the SW South China Sea: Basin Research, v. 26, no. 1, p. 106-134.

Liang, Y., Delescluse, M., Qiu, Y., Pubellier, M., Chamot-Rooke, N., Wang, J., Nie, X., Watremez, L., Chang, S. P., Pichot, T., Savva, D., and Meresse, F., 2019, Décollements,

725 detachments and rafts in the extended crust of Dangerous Ground, South China Sea: the role
726 of inherited contacts: Tectonics, v. 38, no. 6, p. 1863-1883.
727 Ligi, M., Bonatti, E., Bosworth, W., Cai, Y., Cipriani, A., Palmiotto, C., Ronca, S., and Seyler,
728 M., 2018, Birth of an ocean in the Red Sea: Oceanic-type basaltic melt intrusions precede
729 continental rupture: Gondwana Research, v. 54, p. 150-160.
730 Lister, G.S., Etheridge, M. a, Symonds, P. a, 1986. Detachment faulting and the evolution of
731 passive continental margins Detachment faulting and the evolution of passive continental
732 margins. Geology 14, 246–250. https://doi.org/10.1130/0091-7613(1986)14<246
733 Lü, C., Hao, T., Lin, J., and Qiu, X., 2016, The role of rifting in the development of the
734 continental margins of the southwest subbasin, South China Sea: Insights from an OBS
735 experiment: Marine Geophysical Research, p. 1-19.
736 Lunt, P., 2019, A new view of integrating stratigraphic and tectonic analysis in South China
737 Sea and north Borneo basins: Journal of Asian Earth Sciences, v. 177, p. 220-239.
738 Luo, P., Manatschal, G., Ren, J., Zhao, Z., Wang, H., and Tong, D., 2021, Tectono - Magmatic
739 and stratigraphic evolution of final rifting and breakup: Evidence from the tip of the
740 southwestern propagator in the south China sea: Marine and Petroleum Geology, v. 129.
741 Madon, M., Kim, C. L., and Wong, R., 2013, The structure and stratigraphy of deepwater
742 Sarawak, Malaysia: Implications for tectonic evolution: Journal of Asian Earth Sciences, v.
743 76, p. 312-333.
744 Maraquis, G., Roques, D., Huchon, P., Coulon, O., Chamot-Rooke, N., Rangin, C., and Le
745 Pichon, X., 1997, Amount and timing of extension along the continental margin off central
746 Vietnam: Bull. Soc. géol. Fr, v. 168, no. 6, p. 707-716.
747 McIntosh, K., Lavier, L., van Avendonk, H., Lester, R., Eakin, D., and Liu, C.-S., 2014, Crustal
748 structure and inferred rifting processes in the northeast South China Sea: Marine and
749 Petroleum Geology, v. 58, p. 612-626.

Mohn, G., Manatschal, G., Beltrando, M., Masini, E., Kusznir, N., 2012. Necking of continental crust in magma-poor rifted margins: Evidence from the fossil Alpine Tethys margins. Tectonics 31, 1–28.

Morley, C. K., 2016, Major unconformities/termination of extension events and associated surfaces in the South China Seas: Review and implications for tectonic development: Journal of Asian Earth Sciences, v. 120, p. 62-86.

Nanni, U., Pubellier, M., Chan, L. S., and Sewell, R. J., 2017, Rifting and reactivation of a Cretaceous structural belt at the northern margin of the South China Sea: Journal of Asian Earth Sciences, v. 136, p. 110-123.

Nirrengarten, M., Manatschal, G., Yuan, X. P., Kusznir, N. J., and Maillot, B., 2016, Application of the critical Coulomb wedge theory to hyper-extended, magma-poor rifted margins: Earth and Planetary Science Letters, v. 442, p. 121-132.

Nirrengarten, M., Mohn, G., Kusznir, N. J., Sapin, F., Despinois, F., Pubellier, M., Chang, S. P., Larsen, H. C., and Ringenbach, J. C., 2020, Extension modes and breakup processes of the southeast China-Northwest Palawan conjugate rifted margins: Marine and Petroleum Geology, v. 113, p. 104123.

Nissen, S.S., Hayes, D.E., Bochu, Y., Zeng, W., Chen, Y., Nu, X., 1995. Gravity, heat flow, and seismic constraints on the processes of crustal extension: Northern margin of the South China Sea. J. Geophys. Res. 100, 22447.

Peng, X., Shen, C., Mei, L., Zhao, Z., and Xie, X., 2018, Rift–drift transition in the Dangerous Grounds, South China Sea: Marine Geophysical Research.

Péron-Pinvidic, G., Manatschal, G., Masini, E., Sutra, E., Flament, J.M., Haupert, I., Unternehr, P., 2017. Unravelling the along-strike variability of the Angola–Gabon rifted margin: a mapping approach. Geol. Soc. London, Spec. Publ. 438, 49–76.

774 Persaud, P., Stock, J. M., Steckler, M. S., Martín-Barajas, A., Diebold, J. B., González-
775 Fernández, A., and Mountain, G. S., 2003, Active deformation and shallow structure of the
776 Wagner, Consag, and Delfín Basins, northern Gulf of California, Mexico: Journal of
777 Geophysical Research: Solid Earth, v. 108, no. B7.
778 Pichot, T., Delescluse, M., Chamot-Rooke, N., Pubellier, M., Qiu, Y., Meresse, F., Sun, G.,
779 Savva, D., Wong, K. P., Watremez, L., and Auxiètre, J. L., 2014, Deep crustal structure of
780 the conjugate margins of the SW South China Sea from wide-angle refraction seismic data:
781 Marine and Petroleum Geology, v. 58, Part B, p. 627-643.
782 Pubellier, M., Chang S-P, Delescluse M, 2021, The South China Sea; Rifting Peculiarities of a
783 Marginal Basin, Special Volume "Continental Margins" Willey Eds.
784 Qiu, Y., Wang, Y., Huang, W., Li, W., Zhuo, H., Du, W., and Gong, C., 2016, Jump event of
785 mid-ocean ridge during the eastern subbasin evolution of the South China Sea: Interpretation,
786 v. 4, no. 3, p. SP67-SP77.
787 Rangin, C., 1989. The Sulu Sea, a back-arc basin setting within a Neogene collision zone.
788 Tectonophysics, 161(1-2): 119-141.
789 Ranero, C.R., Pérez-Gussinyé, M., 2010. Sequential faulting explains the asymmetry and
790 extension discrepancy of conjugate margins. Nature 468, 294–299.
791 Reston, T.J., 2009. The structure, evolution and symmetry of the magma-poor rifted margins
792 of the North and Central Atlantic: A synthesis. Tectonophysics 468, 6–27.
793 Ros, E., Pérez-Gussinyé, M., Araújo, M., Thoaldo Romeiro, M., Andrés-Martínez, M., and
794 Morgan, J. P., 2017, Lower Crustal Strength Controls on Melting and Serpentinization at
795 Magma-Poor Margins: Potential Implications for the South Atlantic: Geochemistry,
796 Geophysics, Geosystems, v. 18, no. 12, p. 4538-4557.

797 Roques, D., Ranero, C., and Huchon, P., 1997, Geometry and sense of motion along the
798 Vietnam continental margin: onshore/offshore Da Nang area: Bull. Soc. géol. Fr, v. 168, no.
799 4, p. 413-422.
800 Ru, K., Pigott, J.D., 1986. Episodic rifting and subsidence in the South China Sea. AAPG
801 Bulletin, 70(9): 1136-1155.
802 Sapin, F., Ringenbach, J. C., and Clerc, C., 2021, Rifted margins classification and forcing
803 parameters: Sci Rep, v. 11, no. 1, p. 8199.
804 Savva, D., Meresse, F., Pubellier, M., Chamot-Rooke, N., Lavier, L., Po, K. W., Franke, D.,
805 Steuer, S., Sapin, F., Auxietre, J. L., and Lamy, G., 2013, Seismic evidence of hyper-
806 stretched crust and mantle exhumation offshore Vietnam: Tectonophysics, v. 608, p. 72-83.
807 Savva, D., Pubellier, M., Franke, D., Chamot-Rooke, N., Meresse, F., Steuer, S., and Auxietre,
808 J. L., 2014, Different expressions of rifting on the South China Sea margins: Marine and
809 Petroleum Geology, v. 58, no. 0, p. 579-598.
810 Schlüter, H. U., Hinz, K., and Block, M., 1996, Tectono-stratigraphic terranes and detachment
811 faulting of the South China Sea and Sulu Sea: Marine Geology, v. 130, no. 1-2, p. 39-78.
812 Sewell, R.J., Campbell, S.D.G., 1997. Geochemistry of coeval Mesozoic plutonic and volcanic
813 suites in Hong Kong. Journal of the Geological Society, London, 154: 1053-1066.
814 Sibuet, J. C., Yeh, Y. C., and Lee, C. S., 2016, Geodynamics of the South China Sea:
815 Tectonophysics, v. 692, p. 98-119.
816 Song, T., and Li, C.-F., 2015, Rifting to drifting transition of the Southwest Subbasin of the
817 South China Sea: Marine Geophysical Research, v. 36, no. 2-3, p. 167-185.
818 Song, T., Li, C.-F., Wu, S., Yao, Y., and Gao, J., 2019, Extensional styles of the conjugate rifted
819 margins of the South China Sea: Journal of Asian Earth Sciences, v. 177, p. 117-128.
820 Steuer, S., Franke, D., Meresse, F., Savva, D., Pubellier, M., and Auxietre, J.-L., 2014,
821 Oligocene–Miocene carbonates and their role for constraining the rifting and collision

history of the Dangerous Grounds, South China Sea: Marine and Petroleum Geology, v. 58, Part B, no. 0, p. 644-657.

Su, D., White, N., McKenzie, D., 1989. Extension and subsidence of the Pearl River mouth basin, northern South China Sea. Basin Research, 2: 205-222.

Sutra, E., Manatschal, G., Mohn, G., Unternehr, P., 2013. Quantification and restoration of extensional deformation along the Western Iberia and Newfoundland rifted margins. Geochemistry, Geophys. Geosystems 14, 2575–2597.

Sun, Q., Wu, S., Cartwright, J., Lüdmann, T., and Yao, G., 2013, Focused fluid flow systems of the Zhongjiannan Basin and Guangle Uplift, South China Sea: Basin Research, v. 25, no. 1, p. 97-111.

Taylor, B., and Hayes, D. E., 1980, The tectonic evolution of the South China Basin, v. 23, p. 89-104.

Taylor, B., Hayes, DE, 1983. Origin and history of the South China Sea basin, in: Hayes, Dennis (Ed.), The Tectonic and Geologic Evolution of Southeast Asian Seas and Islands: Part 2. pp. 23–56.

Teng, L. S., and Lin, A. T., 2004, Cenozoic tectonics of the China continental margin: insights from Taiwan: Geological Society, London, Special Publications, v. 226, no. 1, p. 313-332.

Tetreault, J. L., and Buiter, S. J. H., 2018, The influence of extension rate and crustal rheology on the evolution of passive margins from rifting to break-up: Tectonophysics, v. 746, p. 155-172.

Tong, D., Ren, J., Liao, Y., Yao, Y., and Zhao, Y., 2019, Cenozoic tectonic events and their implications for constraining the structure and stratigraphic styles from rifting to collision at the southeastern margin of the South China Sea: Marine Geophysical Research, v. 40, no. 2, p. 145-161.

Tugend, J., Gillard, M., Manatschal, G., Nirrengarten, M., Harkin, C., Epin, M.-E., Sauter, D., Autin, J., Kusznir, N., and McDermott, K., 2018, Reappraisal of the magma-rich versus magma-poor rifted margin archetypes: Geological Society, London, Special Publications.

Van Hinsbergen, D.J.J., Vissers, R.L.M., Spakman, W., 2014. Origin and consequences of western Mediterranean subduction, rollback, and slab segmentation. Tectonics 33, 393–419.

Vu, A. T., Wessel Fyhn, M. B., Xuan, C. T., Nguyen, T. T., Hoang, D. N., Pham, L. T., and Van, H. N., 2017, Cenozoic tectonic and stratigraphic development of the Central Vietnamese continental margin: Marine and Petroleum Geology, v. 86, p. 386-401.

Wang, D. W., Wu, S. G., Qin, Z. L., Spence, G., and Lu, F. L., 2013, Seismic characteristics of the Huaguang mass transport deposits in the Qiongdongnan Basin, South China Sea: Implications for regional tectonic activity: Marine Geology, v. 346, p. 165-182.

Wang, Y., Qiu, Y., Yan, P., Zheng, H., Liu, H., and Wang, J., 2016, Seismic evidence for Mesozoic strata in the northern Nansha waters, South China Sea: Tectonophysics, v. 677-678, p. 190-198.

Xiao, H., Dahlen, F.A., Suppe, J., 1991. Mechanics of extensional wedges. J. Geophys. Res. 96, 10301. http://dx.doi.org/10.1029/91JB00222.

Xiao, M., Yao, Y.-J., Cai, Y., Qiu, H.-N., Xu, Y.-G., Xu, X., Jiang, Y.-D., Li, Y.-B., Xia, X.-P., and Yu, Y.-J., 2019, Evidence of Early Cretaceous lower arc crust delamination and its role in the opening of the South China Sea: Gondwana Research, v. 76, p. 123-145.

Xie, X., Müller, R. D., Li, S., Gong, Z., and Steinberger, B., 2006, Origin of anomalous subsidence along the Northern South China Sea margin and its relationship to dynamic topography: Marine and Petroleum Geology, v. 23, no. 7, p. 745-765.

Xie, X., Ren, J., Pang, X., Lei, C., and Chen, H., 2019, Stratigraphic architectures and associated unconformities of Pearl River Mouth basin during rifting and lithospheric breakup of the South China Sea: Marine Geophysical Research.

871 Yan, P., Zhou, D., and Liu, Z., 2001, A crustal structure profile across the northern continental
872 margin of the South China Sea: Tectonophysics, v. 338, no. 1, p. 1-21.
873 Yan, Q., Shi, X., Liu, J., Wang, K., and Bu, W., 2010, Petrology and geochemistry of Mesozoic
874 granitic rocks from the Nansha micro-block, the South China Sea: Constraints on the
875 basement nature: Journal of Asian Earth Sciences, v. 37, no. 2, p. 130-139.
876 Yao, Y., Liu, H., Yang, C., Han, B., Tian, J., Yin, Z., Gong, J., and Xu, Q., 2012, Characteristics
877 and evolution of Cenozoic sediments in the Liyue Basin, SE South China Sea: Journal of
878 Asian Earth Sciences, v. 60, p. 114-129.
879 Ye, Q., Mei, L., Shi, H., Shu, Y., Camanni, G., and Wu, J., 2018, A low-angle normal fault and
880 basement structures within the Enping Sag, Pearl River Mouth Basin: Insights into late
881 Mesozoic to early Cenozoic tectonic evolution of the South China Sea area: Tectonophysics,
882 v. 731-732, p. 1-16
883 Zhang, G., Shao, L., Qiao, P., Cao, L., Pang, X., Zhao, Z., Xiang, X., Cui, Y., and Li, S., 2019,
884 Cretaceous–Palaeogene sedimentary evolution of the South China Sea region: A preliminary
885 synthesis: Geological Journal.
886 Zhang, J., Wu, Z., Shen, Z., Dong, C., Wang, C., and Zhao, Y., 2020a, Seismic evidence for
887 the crustal deformation and kinematic evolution of the Nansha Block, South China Sea:
888 Journal of Asian Earth Sciences, v. 203.
889 Zhang, Y., Xia, S., Cao, J., Zhao, F., Fan, C., Xu, H., and Wan, K., 2020b, Extensional tectonics
890 and post-rift magmatism in the southern South China Sea: New constraints from multi-
891 channel seismic data: Marine and Petroleum Geology, v. 117, p. 104396.
892 Zhao, F., Alves, T. M., Wu, S., Li, W., Huuse, M., Mi, L., Sun, Q., and Ma, B., 2016, Prolonged
893 post-rift magmatism on highly extended crust of divergent continental margins (Baiyun Sag,
894 South China Sea): Earth and Planetary Science Letters, v. 445, p. 79-91.

Zwaan, F., Schreurs, G., and Rosenau, M., 2020, Rift propagation in rotational versus orthogonal extension: Insights from 4D analogue models: Journal of Structural Geology, v. 135, p. 103946.

Table captions

Table 1. Acquisition parameters of seismic lines.

Seismic line	CFT		NGH-1-3*	INL320*
Year	2011, 2013		2009	2011
Source energy (cubic inch)	~7000	~7000	5080	5080
Streamer channel	640	480	480	480
Receiver interval (m)	12.5	12.5	12.5	12.5
Shot interval (m)	50	50	37.5	37.5
Record length (sec)	16	16	12	12
Sample rate (ms)	2	2	2	2

*Parameters routinely used by GMGS for data acquisition and processing in the SCS.

Figure captions

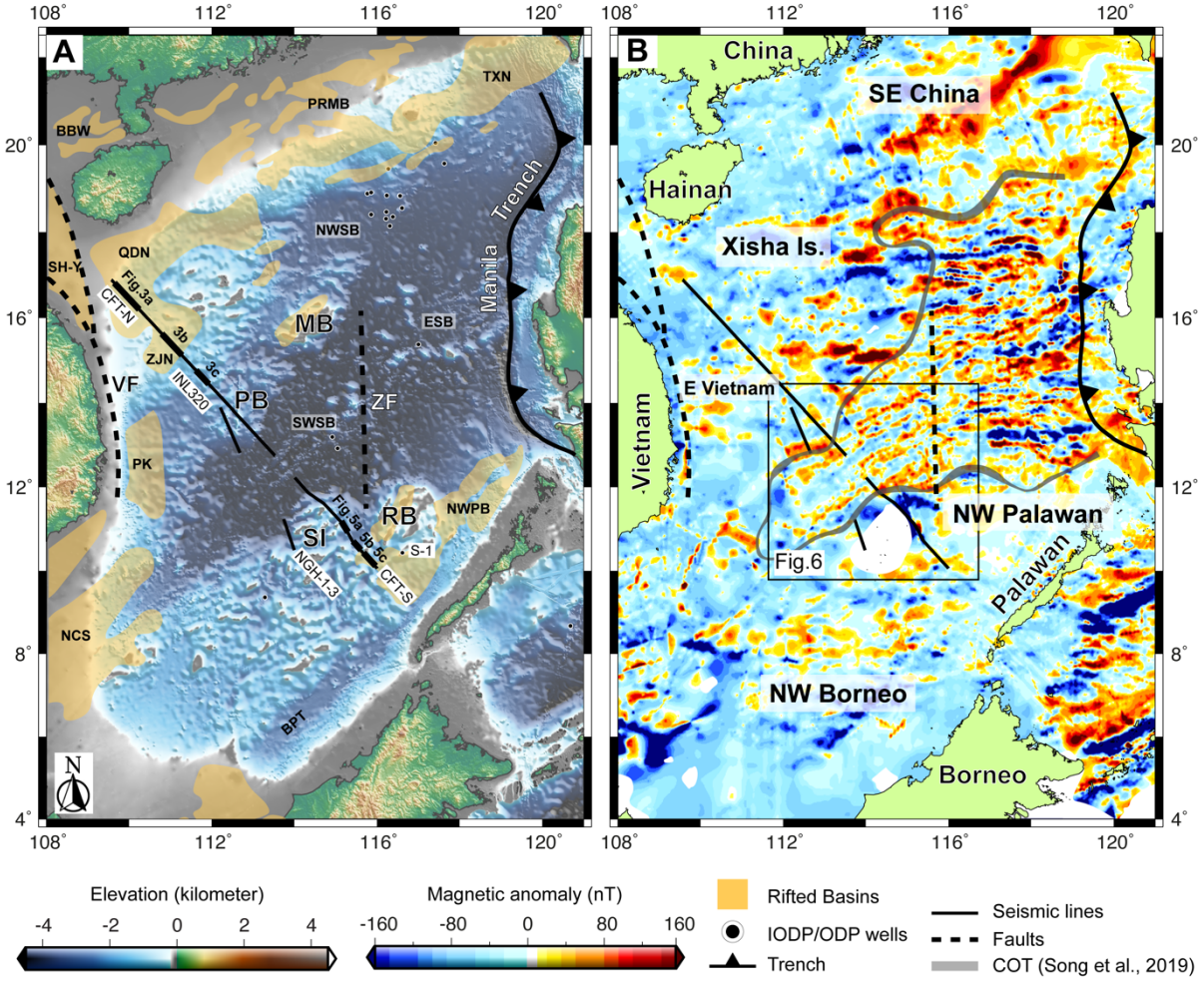

Figure 1. (A) Elevation with rifted basins including BBW: Beibuwan Basin, NCS: Nam Con Son Basin, NWPB: NW Palawan Basin, PK: Phu Khanh Basin, PRMB: Pearl River Mouth

Basin, QDN: Qiongdongnan Basin, SH-Y: Song Hong-Yinggehai Basin, TXN: Taixinan Basin, ZJN: Zhongjiannan Basin. The bathymetric map has a non-linear colour bar to assist in highlighting certain features. The black solid lines represent the location of seismic profiles and the black dashed lines are Vietnam Fault (VF) and Zhongnan Fault (ZF) (Fyhn et al., 2009; Li et al., 2015). (B) Marine magnetic anomaly map. The magnetic map is compiled by Geological Survey of Japan and CCOP (1996). The white area represents areas devoid of data. The COT distribution is shown in the grey band (Song et al., 2019). MB: Macclesfield Bank (Zhongsha Islands), SI: Spratly (Nansha) Islands, PB: Penxi Bank, RB: Reed (Liyue) Bank. ESB: East Sub-Basin, NWSB: Northwest Sub-Basin, SWSB: Southwest Sub-Basin, BPT: Borneo-Palawan Trough.

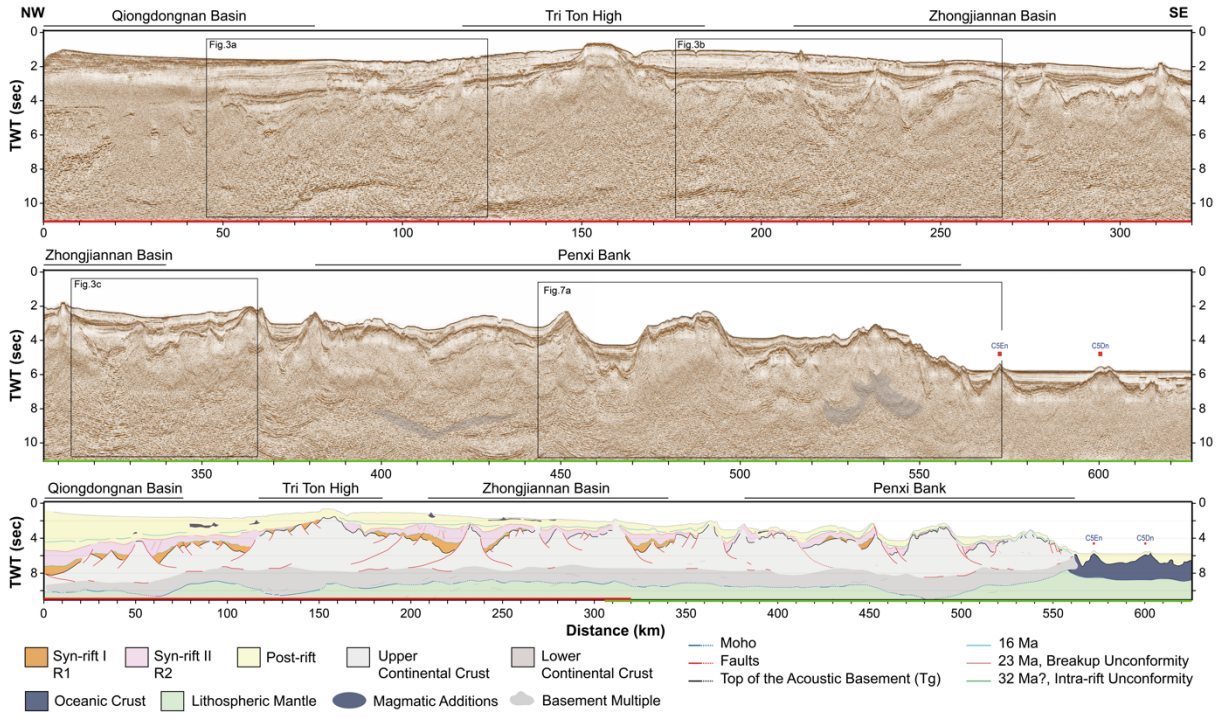

Figure 2. Original and interpreted seismic profiles of ENS processed line CFT-N across the Xisha Islands Margin. The wide rifted margin is characterized by distributed basins with two phases of syn-rift units, which are bounded by detachment faults. The location is shown on the Fig.1.

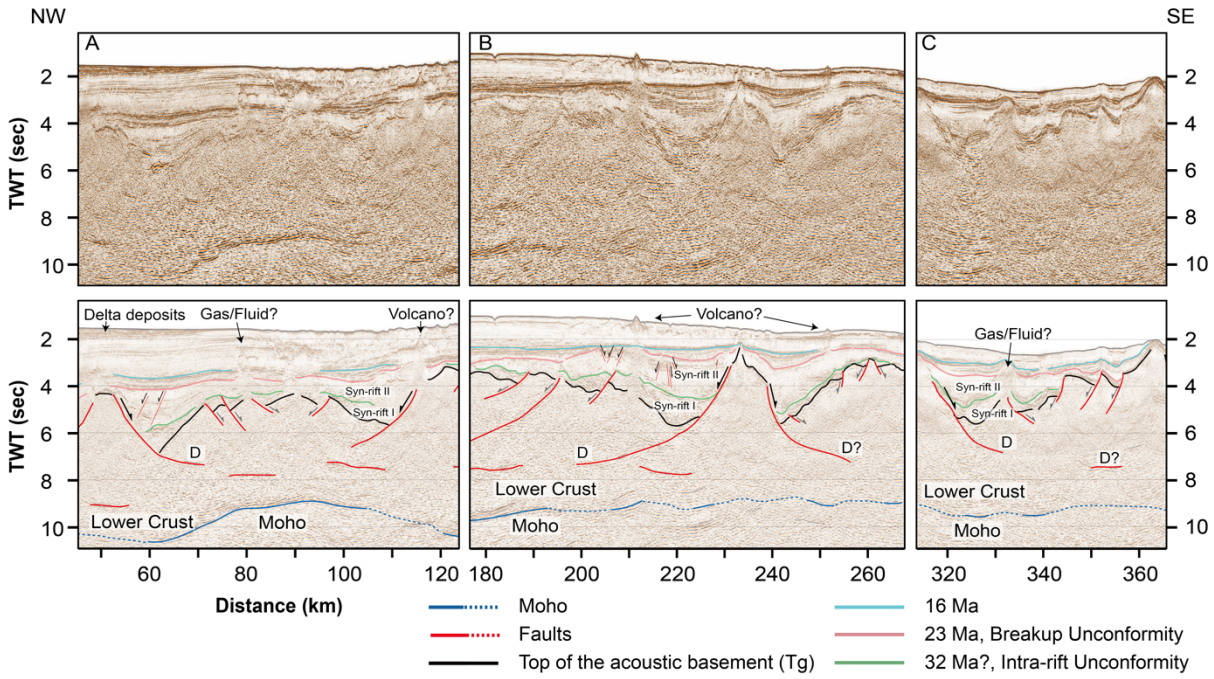

Figure 3. Original and interpreted seismic profiles, showing the extended crust in the Qiongdongnan Basin and Zhongjiannan Basin showing that the detachment faults (D) thin mainly the crust and root into the top of the lower crust. The Moho depth follows weak reflectivity and refraction Moho from Pichot et al. (2014). Vertical exaggeration is approximately 5 in the sediments and 2 in the crust, based on refraction data such as the average velocity 2 km/s for sediments and 6.5 km/s for the continental crust. The location is shown on Fig.1a and in Fig.2.

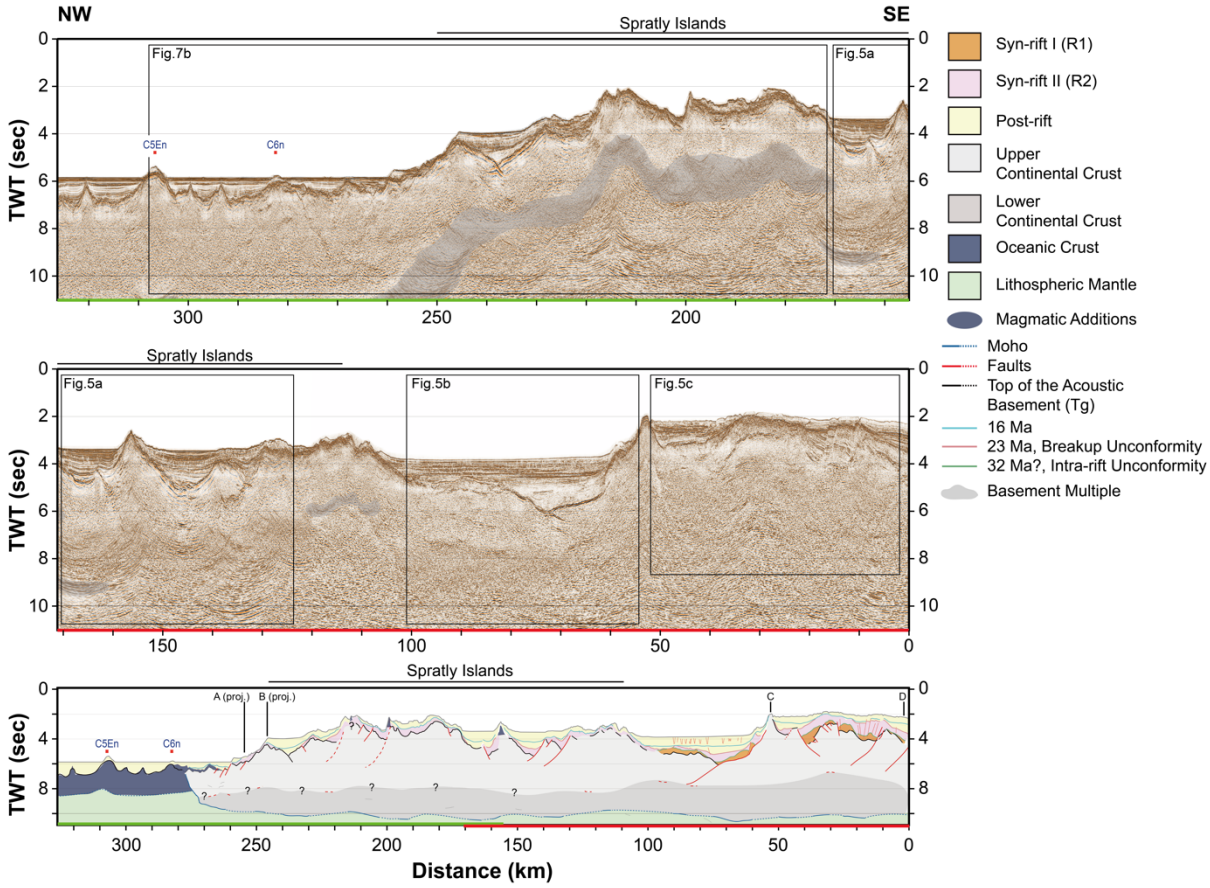

Figure 4. Original and interpreted seismic profiles of line CFT-S across the NW Borneo Margin with the indication of dredge samples along the profile. A: monzo-granite and granodiorite (127.2-153.6 Ma); B: tonalite (157.8-159.1 Ma); C: gneiss (115-123 Ma) and phyllite (113 Ma); D: lagoonal-reefoid packstone-wackestone (E. Miocene) (Kudrass et al., 1986; Yan et al., 2012). The location of the seismic profile is shown on Fig.1 and sample locations are shown on Fig.6.

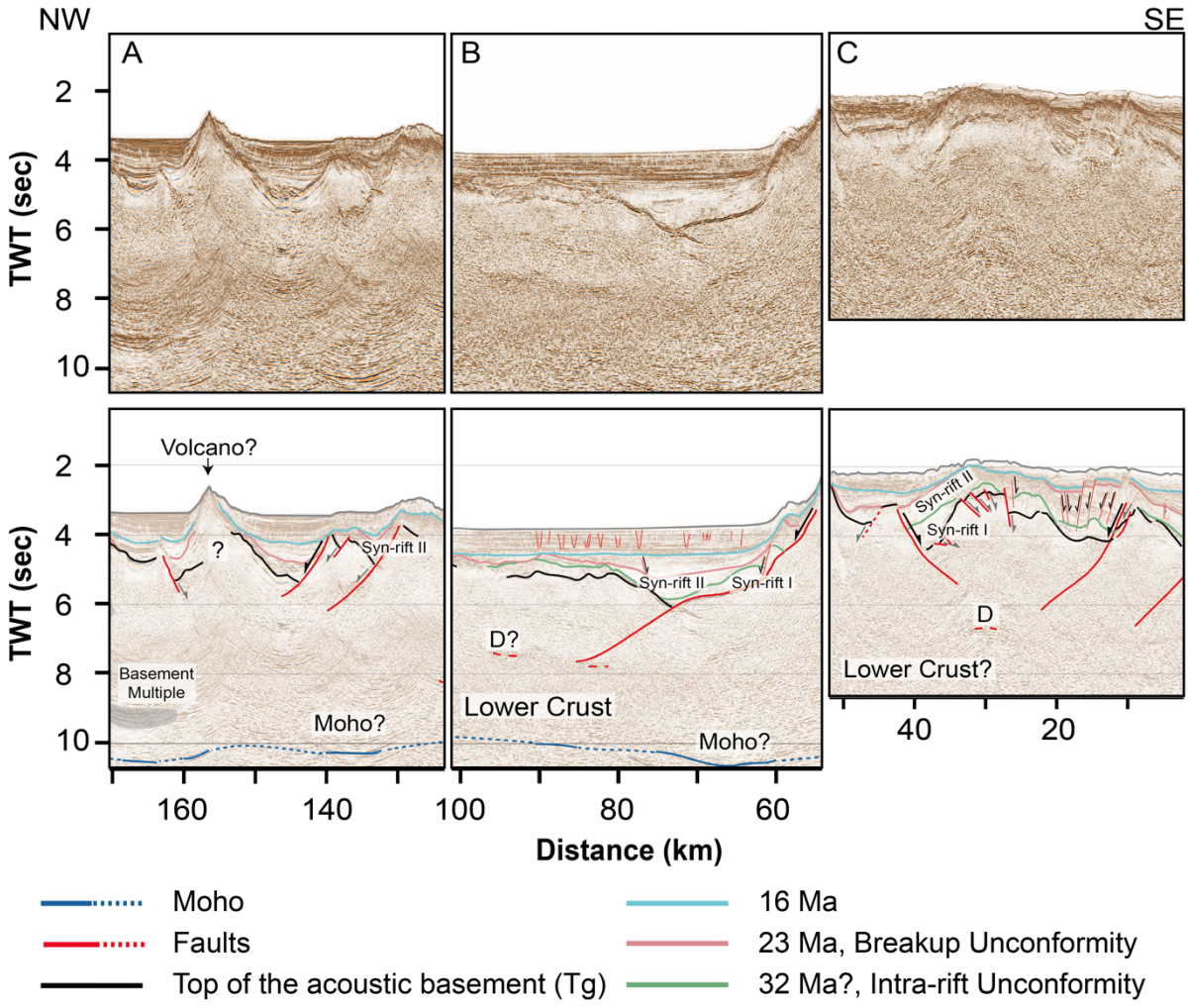

942

943 **Figure 5.** Original and interpreted seismic profile of the extended crust in the area of the Spratly
944 Islands showing the detachment faults (D) rooting in the lower crust and creating the wedge-
945 shaped syn-rift unit in the NW Borneo Margin. The Moho depth follows weak reflectivity and
946 refraction Moho from Liang et al. (2019). Vertical exaggeration is approximately 5 in the
947 sediments and 2 in the crust, estimated by the velocity 2 km/s for sediments and 6.5 km/s for
948 the continental crust. The location is shown on the Fig.1a.

949

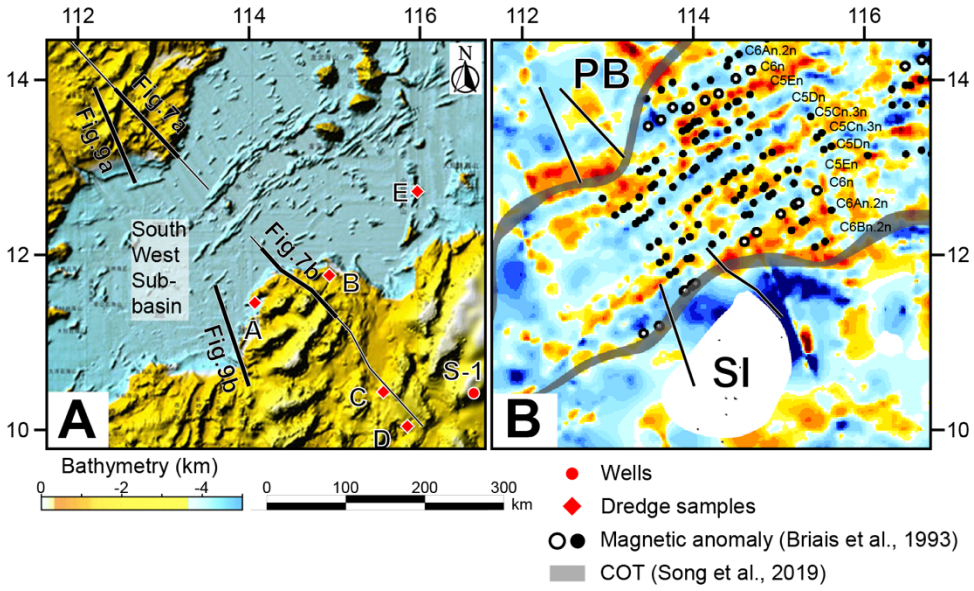

950 **Figure 6.** (A) Bathymetry map in Penxi Bank (PB) and Spratly Islands (SI) in the southwestern SCS. The
951 yellow to blue bathymetry threshold shows two orientations (E-W and N-S) segmenting the
952 continent-ocean transition at the boundary of PB and SI. Two cross-sections present the crustal
953 architecture of conjugated margins by juxtaposing the E Vietnam Margin and NW Borneo
954 Margin along two segments individually. S-1: Well Sampaguita-1. (B) The magnetic anomaly
955 map shows the ages of oceanic crust identified by Briais et al. (1993). The open circle represents
956 the C6n, which is the first anomaly along the seismic profiles. The reconstruction of the
957 conjugated margins are established based on the C5En in this study.
958
959

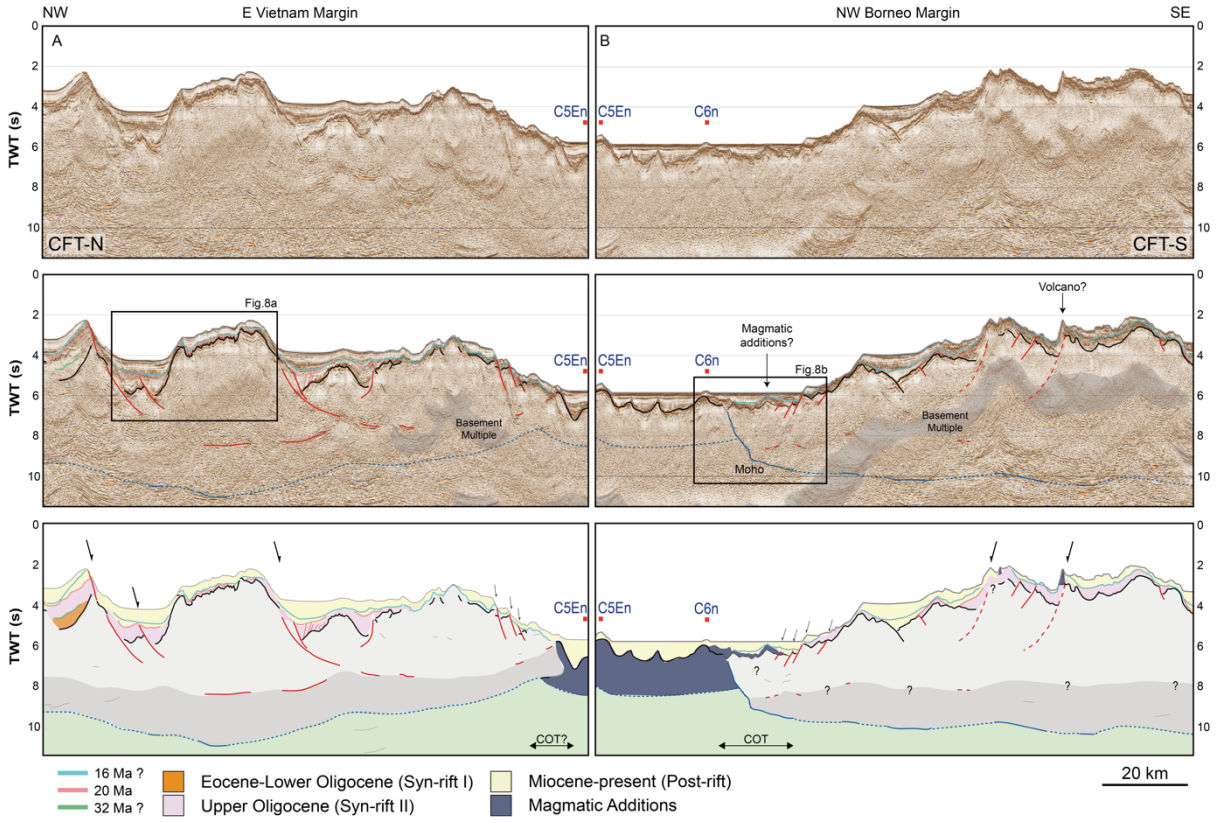

960

961 **Figure 7.** Seismic profiles of a conjugated cross-section along the N-S segment present the
962 thinned crust covered by thin syn-rift sediment at the time of breakup (C6n, 20.1 Ma). The
963 location of the profiles is shown in Fig.6a.

964

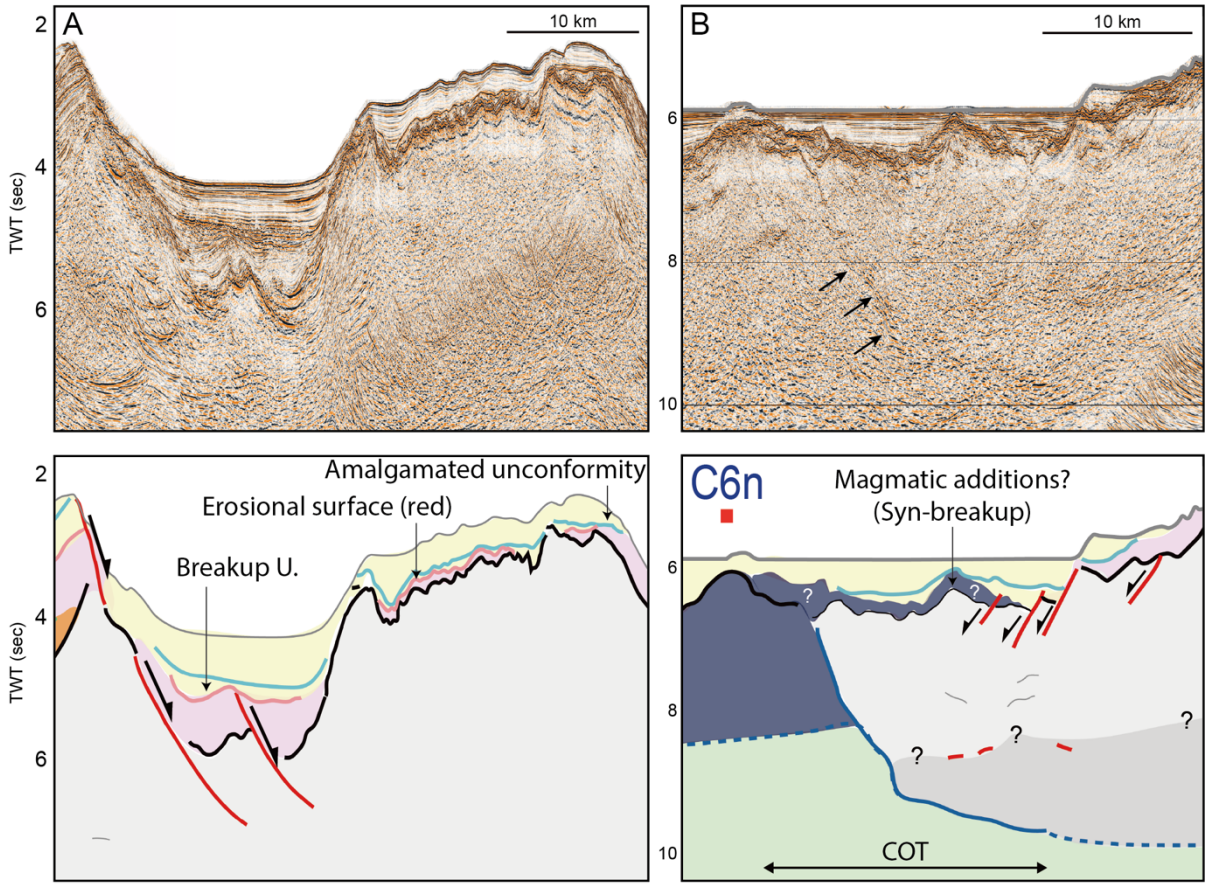

965

966 **Figure 8.** Seismic profiles of rifted basins illustrate (A) an erosional surface (red color)
967 distributed along the rifted basins and basement high in the N-S segment and (B) a thin syn-rift
968 succession covering the COT area.

969

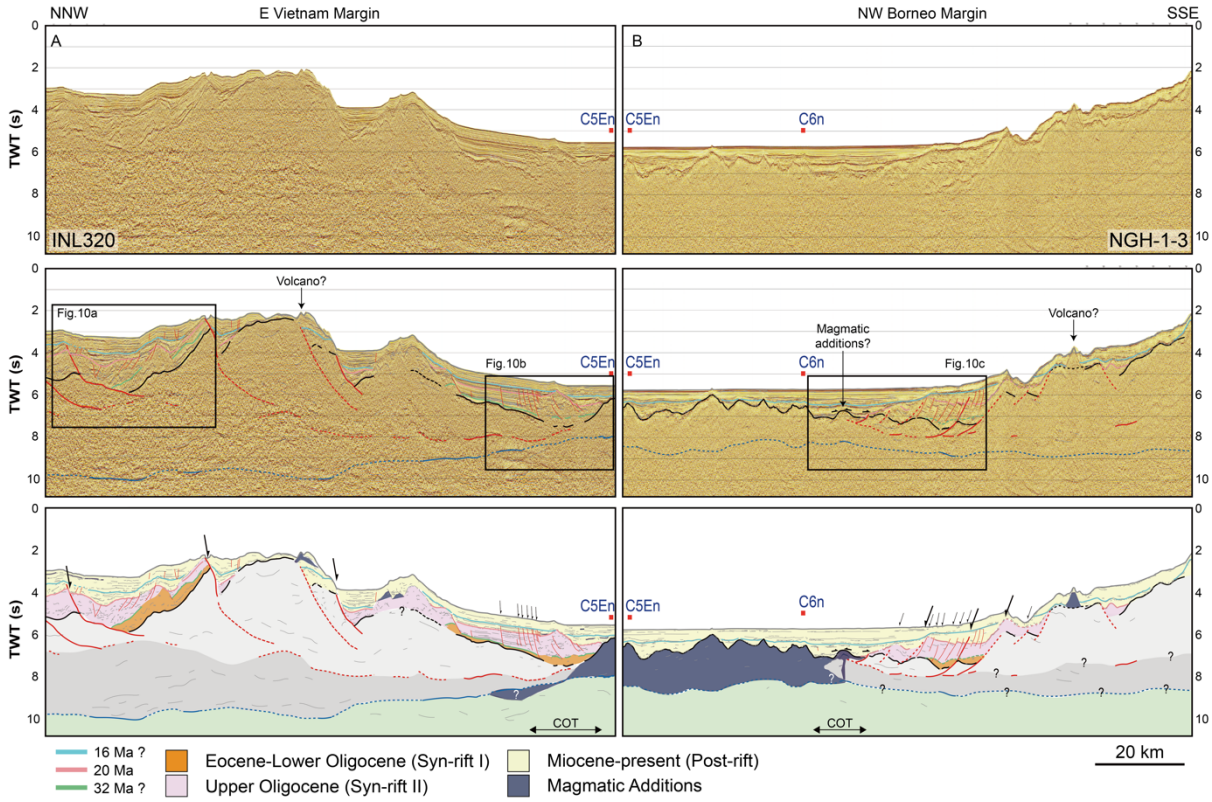

970

971 **Figure 9.** Original and interpreted seismic profile of a conjugated cross-section along the E-W

972 segment presents the thick syn-rift sediment at the time of breakup (C6n, 20.1 Ma). The location

973 of profiles is shown in Fig.6a.

974

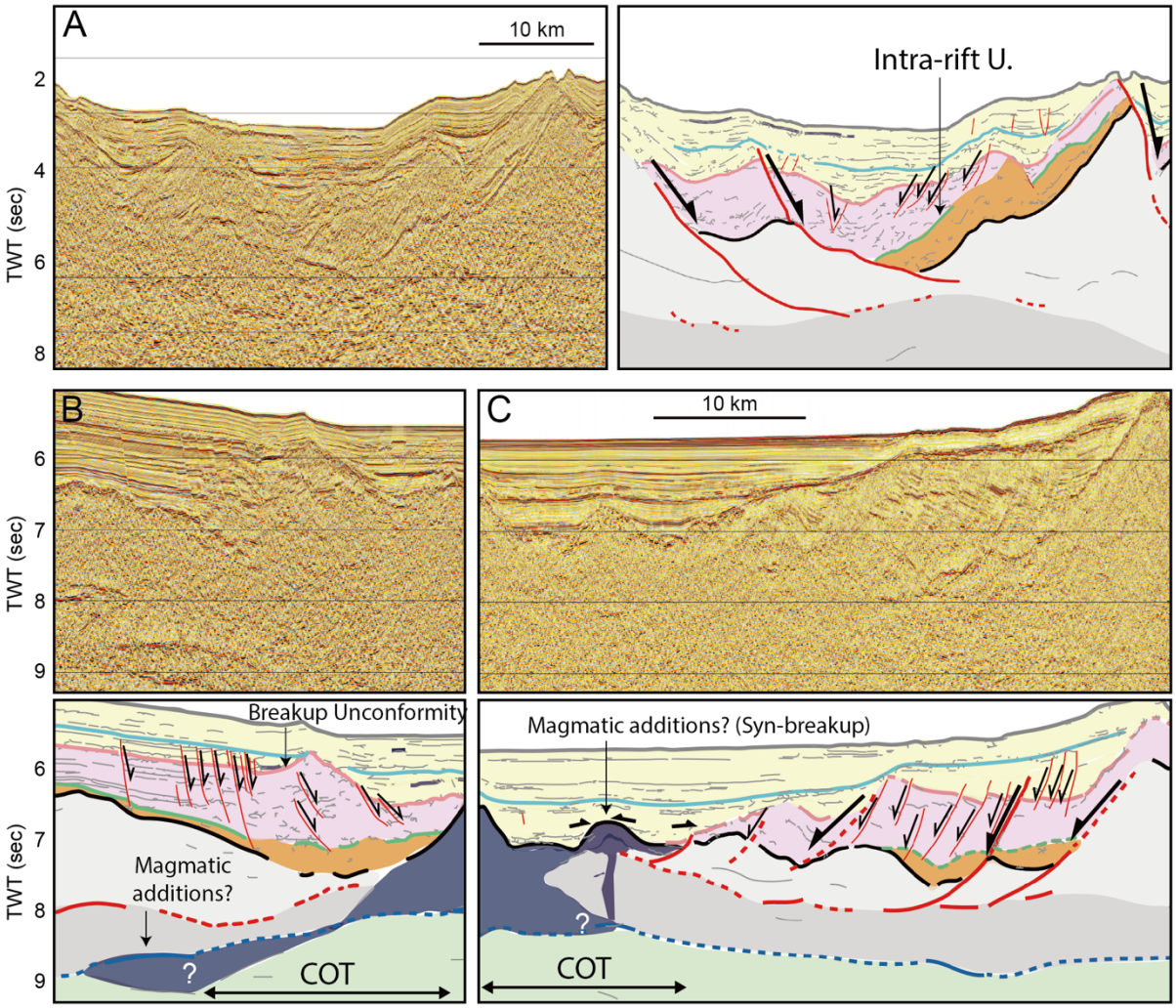

975

976 **Figure 10.** Seismic profiles show that thicker sediments cover the COT of E-W segment in a
977 homogeneous thickness of the syn-rift II succession. The syn-rift unit next to the oceanic crust
978 was disturbed and truncated to form the break-up unconformity. It is suspected that the green
979 horizons (32 Ma) act as a decoupling level which facilitated the tilting of the overlying sequence
980 (Syn-rift II, pink color).

981

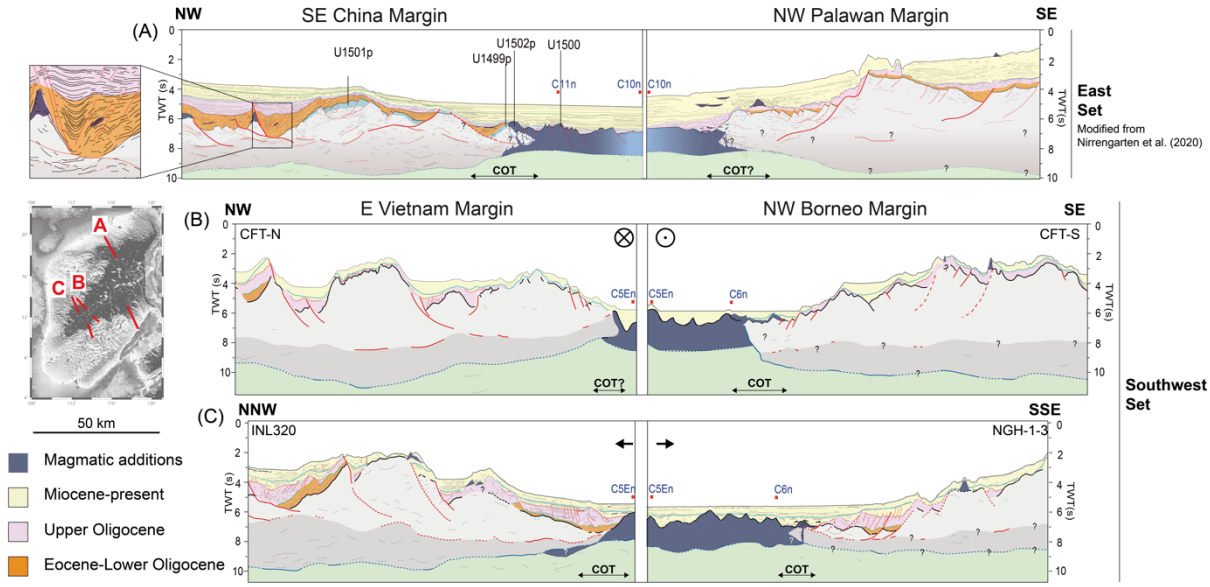

Figure 11. The comparison of crustal configuration between East and Southwest SCS. The wrench component leads the N-S segment (section B) prior to the breakup. The pull-apart basin along the E-W segment (section C) deposited thicker syn-rift sediment. Different ages of breakup and breakup unconformity are presented between E Vietnam-NW Borneo Margin and SE China-NW Palawan Margin, modified from Nirrengarten et al. (2020). The similarity of asymmetrical structure appears near the COT.

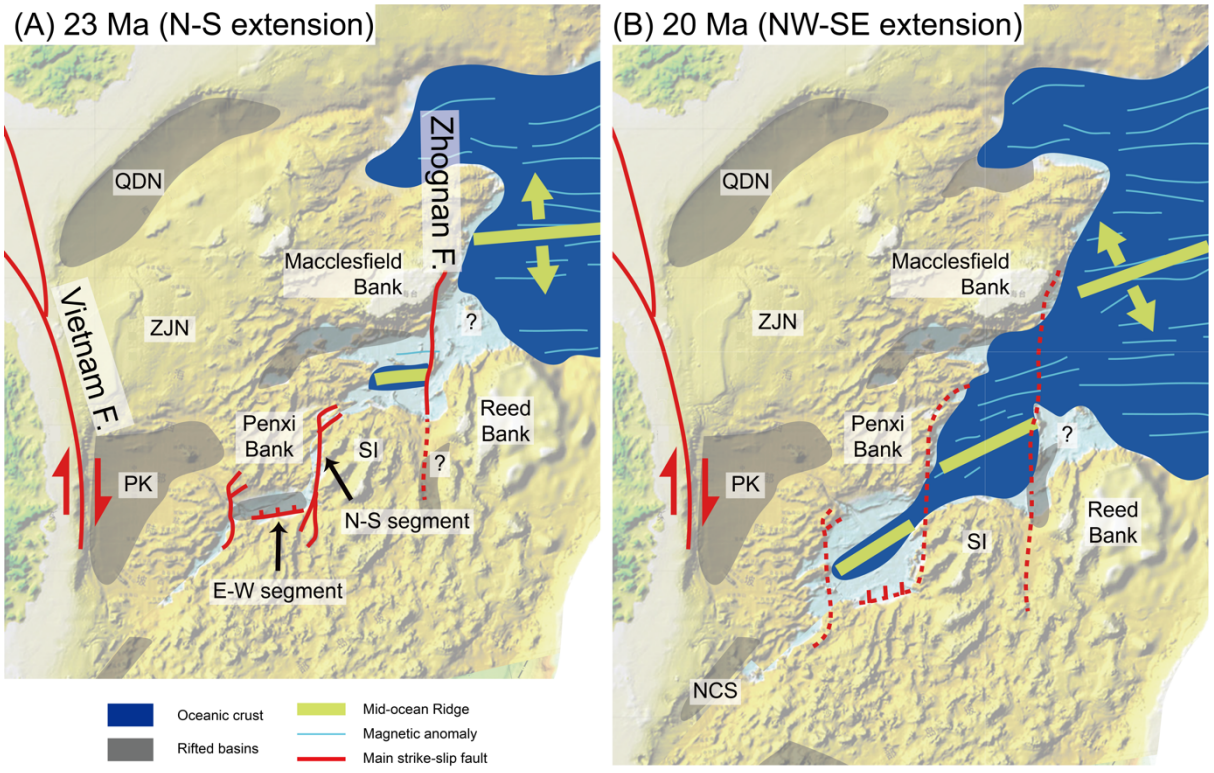

990

991 **Figure 12.** The kinematic evolution in the SCS shows that the first phase of seafloor spreading
992 induced a series of pull-apart basins in the southwestern SCS in a N-S extension and that the
993 second phase changed the direction of seafloor spreading and initiated breakup and subsequent
994 NW-SE spreading.

995

996

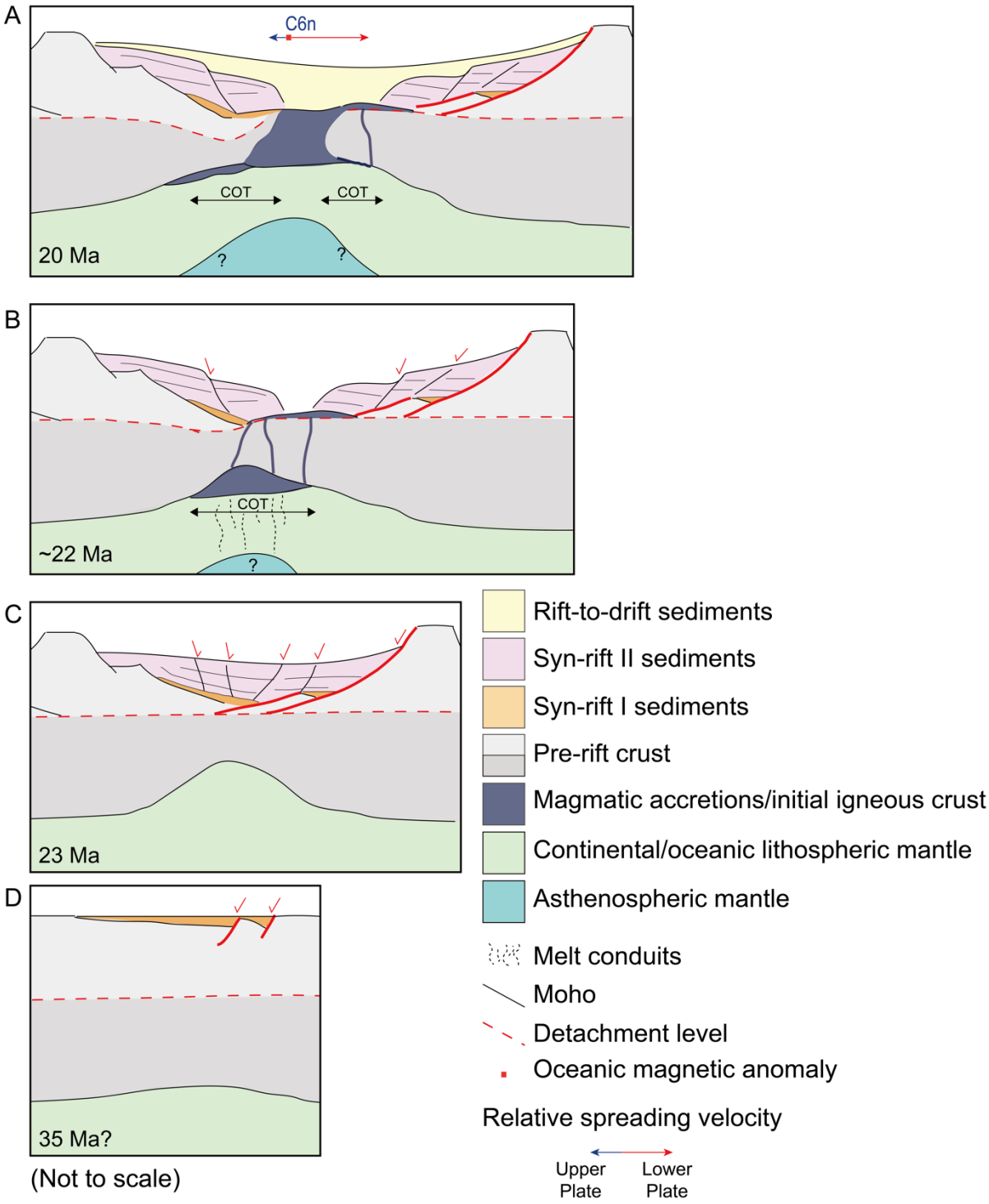

997

998 **Figure 13.** Conceptual model of breakup in the southwestern SCS. Detachment faults attempted

999 to exhume lower structural levels asymmetrically, and were followed by oceanic accretion

1000 which formed the first anomaly (C6n) in the south.

1001

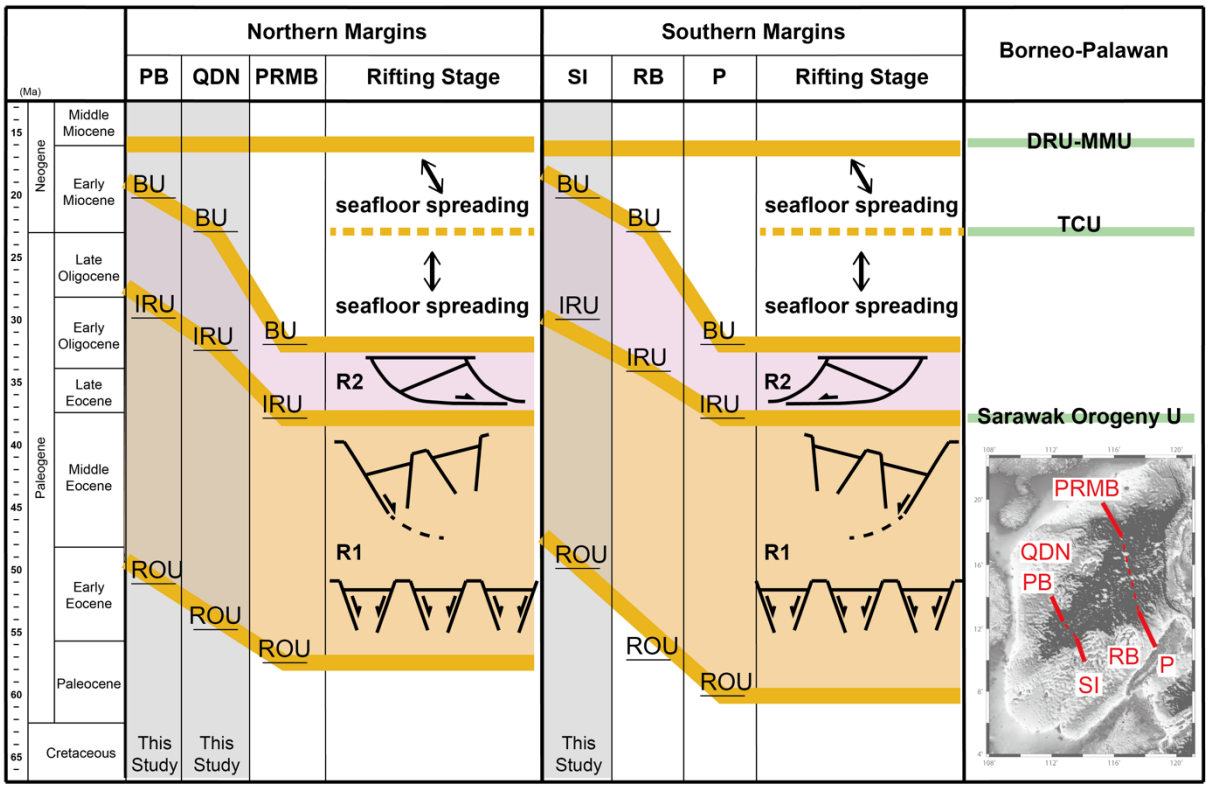

Figure 14. Tectono-stratigraphic chart in diachronism along the SCS margins. Note that the pink and orange colors correspond to the structural stages discussed in the text. In that sense, they do not refer to specific ages of each basin. Ages of the unconformities are taken from Cullen (2010), Yao et al. (2012), Madon et al. (2013), Savva et al. (2013), Steuer et al. (2014), Vu et al. (2017), Xie et al. (2019). The development of detachment faults and breakup results from the two stages of structural evolution in R1 and R2, and shows the various timing along the margin. BU: Breakup Unconformity, IRU: Intra-rift Unconformity, ROU: Rift-onset Unconformity, DRU: Deep-region Unconformity, MMU: Middle Miocene Unconformity, TCU: Top Croker Unconformity.